



RESEARCH MEMORANDUM

TRANSONIC WIND-TUNNEL INVESTIGATION OF THE INTERFERENCE
BETWEEN A 45° SWEEPBACK WING AND A SYSTEMATIC
SERIES OF FOUR BODIES

By Donald L. Loving and Dewey E. Wornom

Langley Aeronautical Laboratory
Langley Field, Va.

NATIONAL ADVISORY COMMITTEE
FOR AERONAUTICS
WASHINGTON

November 20, 1952
Declassified October 18, 1956

NATIONAL ADVISORY COMMITTEE FOR AERONAUTICS

RESEARCH MEMORANDUM

TRANSONIC WIND-TUNNEL INVESTIGATION OF THE INTERFERENCE
BETWEEN A 45° SWEEPBACK WING AND A SYSTEMATIC
SERIES OF FOUR BODIES

By Donald L. Loving and Dewey E. Wornom

SUMMARY

The interference between a 45° sweptback wing and a systematic series of four bodies has been investigated at subsonic and transonic speeds. Measurements have been made of the aerodynamic characteristics at nonlifting and lifting conditions for the various wing-body configurations and bodies alone at Mach numbers from 0.60 to 1.13 in the Langley 8-foot transonic tunnel. The wing had an aspect ratio of 4, a taper ratio of 0.6, and NACA 65A006 airfoil sections. The original body had a curved profile from the nose to the base; the second had an increased length with a cylindrical midsection between the forebody and boattailed afterbody; the third was the same length as the original body but had a cylindrical afterbody in conjunction with the original forebody; the final configuration was a combination of the second and third modifications, resulting in a cylindrical portion extending from the vicinity of the wing leading edge to the base of the model.

The results obtained revealed that the principal effects of changes in body shape on the interference of the wing and body occurred in the transonic speed range. Drag was most significantly affected by the various body changes. Lift and pitching-moment characteristics up to the highest angles of attack tested were little affected by the body changes. The zero-lift drag rise of the wing with interference associated with the original curved afterbody was reduced 50 percent by the use of the cylindrical afterbody in combination with the wing at a Mach number of 1.00. The maximum lift-drag ratio of the wing with interference was approximately one-third greater at transonic speeds for the wing in combination with the extended forebody and cylindrical afterbody than for the original body. The results also indicated that the modifications had significant effects on the drag characteristics of the bodies alone at transonic speeds and on the pitching-moment characteristics throughout the complete Mach number range.

INTRODUCTION

Flights are at present being made through the speed of sound with aerodynamic handicaps especially manifest in large changes in the aerodynamic characteristics of the aircraft as the speed of sound is approached. Among the factors affecting the characteristics of airplanes are the properties of the body and the effects of wing-body interference.

This paper discusses some of the results obtained during recent investigations made in the Langley 8-foot transonic tunnel to explore and reduce adverse interference effects of wing-body combinations. The present investigation was made to determine the effects of a few basic changes in body shape on the wing-body interference of a sweptback-wing-body combination. These body changes included an extension of the forebody, the use of a cylindrical midsection between the forebody and afterbody, and a cylindrical afterbody. The discussion deals primarily with the effects of interference on the lift, drag, and pitching moment at transonic Mach numbers since, as will be shown, these effects are most pronounced in this speed range. The major emphasis is placed on the drag characteristics.

The drag of wing-body combinations as well as that of the body alone when subjected to transonic flow is dependent very largely on the presence of shocks associated with induced flow. Such conditions occur, of course, when supersonic velocities are reached on the surface and must go through a deceleration process to reach free-stream conditions downstream. The effect of induced velocities thus becomes of prime importance as the free-stream velocity approaches and passes through the speed of sound. Some discussion of the effect of these induced velocities created by the body alone on its own aerodynamic characteristics is given first. Then, the problem involving the addition of a wing and the subsequent interference of the body on the flow about the wing is analyzed.

Most of the data for the bodies alone and the wing-body combinations were obtained at low angles of attack; however, high-angle-of-attack data were obtained for one of the body modifications. These high-angle-of-attack data are compared with similar data from reference 1 to show the effect of a large body change on the lift and pitch-up tendency of the sweptback wing at moderate to high lifts.

SYMBOLS

C_D drag coefficient, $\frac{D}{qS}$

C_L lift coefficient, $\frac{L}{qS}$

$\frac{\partial C_L}{\partial \alpha}$	lift-curve slope per degree
C_m	pitching-moment coefficient, $\frac{M_{\bar{c}}/4}{qS\bar{c}}$
\bar{c}	wing mean aerodynamic chord
d_{\max}	maximum body diameter
D	drag
L	lift
l	body length
M	Mach number
$M_{\bar{c}}/4$	pitching moment about $0.25\bar{c}$
P_b	base-pressure coefficient, $\frac{P_b - P_o}{q}$
ΔP_b	incremental base-pressure coefficient due to addition of wing to body
p_b	static pressure at base of model
p_o	free-stream static pressure
q	dynamic pressure, $\frac{1}{2}\rho V^2$
R	Reynolds number, based on \bar{c} or l
r	body radius at station x
S	wing area
V	free-stream velocity
x	longitudinal distance from nose of body
α	angle of attack
ρ	free-stream density

APPARATUS AND METHODS

Tunnel

The Langley 8-foot transonic tunnel is a single-return, dodecagonal, slotted-throat wind tunnel which operates at a stagnation pressure approximately equal to atmospheric pressure. The tunnel was capable of continuous operation up to a Mach number of 1.13 for this investigation. A complete description of the Langley 8-foot transonic tunnel may be found in reference 2.

Models

The model combinations investigated had a wing with the quarter-chord line sweptback 45° , an aspect ratio of 4, a taper ratio of 0.6, and NACA 65A006 airfoil sections parallel to the plane of symmetry. The wing was mounted on the bodies in the midwing position. Two wings, differing only in material used in construction, were employed in this investigation. One, used for low-angle-of-attack data, was constructed of 14S-T aluminum alloy and is described in reference 3. The other, used for obtaining high-angle-of-attack data was constructed of steel and is described in reference 1.

The basic body of the combinations, as shown in table I and figure 1, had a fineness ratio of 9.8 and is the same body described and referred to as "fuselage" in reference 1. In the present report this basic body is designated by the letter A, and is further referred to as the body with the original forebody and original afterbody. Three additional bodies were used in the investigations. These were systematic modifications of body A and are designated by the letters B, C, and D. See tables I and II and figure 1. These modifications were made by fixing plastic additions to the forebody and afterbody portions of body A. Body B was developed by extending the original forebody forward a distance equal to twice the maximum diameter of the basic body A and fairing a cylindrical midsection of constant diameter between the forebody shape and the original afterbody. Body C was the result of placing a cylindrical plastic fairing of constant diameter over the original afterbody, making the body cylindrical from the cross section of maximum diameter of the basic body A rearward to the base of the body. The forebody remained the same as the original forebody. Body D was a combination of both the extended forebody used for body B and the cylindrical afterbody used for body C. This modification resulted in a cylindrical section of constant diameter extending over the rear 49 percent of the fuselage length. The ratio of the maximum cross-sectional area of the bodies to the wing area is 0.0606 to 1.0. The longitudinal position of the wing was such that the quarter-chord point of the mean aerodynamic

chord coincided with the station of maximum diameter of the basic body A. Since the length of the afterbody was not varied, the wing remained in the same position relative to the base of the body for all model changes. The surface of the model was maintained in a smooth condition throughout the investigation. Photographs of bodies B and D in combination with the wing are presented as figures 2 and 3.

The basic body was a hollow shell constructed of steel. An electrical strain-gage type of balance was contained within the basic body and secured to the body at its forward end. The rear portion of the balance comprised a sting for supporting the model in the center of the tunnel. For the models with the original afterbody, the sting diverged from the base of the model rearward, as shown in the photograph of body B (fig. 2). The sting rearward from the base of the cylindrical afterbody was cylindrical in cross section with a constant diameter slightly less than that of the body, as shown in figure 3. The sting was secured to a variable-angle-of-attack mechanism controllable from outside the tunnel. Details of the location of the model in the Langley 8-foot transonic tunnel are presented in figure 4.

Tests and Measurements

The investigation was conducted through a Mach number range from 0.6 to 1.13. The angle-of-attack range was from 0° to 7° for all the configurations investigated and also from 0° to 28° for the combination employing both the extended forebody and cylindrical afterbody. Bodies alone were tested as well as wing-body combinations.

The static pressure at the rear of each model was obtained from pressure orifices located in the top and bottom of the sting support in the plane of the model base. These base pressures, together with the base area of the individual models, were used in calculating the base drag coefficients.

The angle of attack of the model was measured by sighting the cross-hair of a cathetometer on a reference line marked on the fuselage. The use of this device in conjunction with the remotely controlled angle-of-attack changing mechanism enabled model angles of attack to be set to within $\pm 0.1^\circ$ with the tunnel operating at any Mach number.

Previous investigations have indicated that wave reflections from the model affected local distributions of pressure on the model. However, as reported in reference 1, the effects of boundary interference on the force and moment characteristics of models similar to the present configurations were small in the Mach number range where boundary-reflected disturbances reached the model. Therefore, data are included throughout the speed range obtainable in the slotted test section and

are not corrected or adjusted for any wave reflections from the tunnel walls.

Consideration of the accuracy of the strain-gage measurements indicated the lift, drag, and pitching-moment coefficients to be approximately within the limits shown in table III. These values are considered the maximum errors possible. The general errors expected for the investigation are believed to be much less.

The average test Reynolds number, based on the mean aerodynamic chord, varied from approximately 1.7×10^6 to 2.2×10^6 . When based on fuselage length, the approximate Reynolds number covered the range between 9.0×10^6 to 13.55×10^6 . (See fig. 5.)

RESULTS

Data for the wing with interference presented herein were obtained by subtracting experimental data for the body from corresponding data for the wing-body combination. The results presented include the interference effect of the wing on the body as well as the interference effect of the body on the wing.

The basic test results for the various body modifications are presented in figure 6 in the form of lift, drag, and pitching-moment coefficient against angle of attack. Data are presented for bodies A, B, and C at angles of attack up to 7° . Data for body D cover the angle-of-attack range from 0° to 28° . The pitching moments were obtained about a point 12.605 inches forward of the base of the model. When the wing was attached to the model, the 0.25-chord-point of the mean aerodynamic chord was in a plane perpendicular to this moment center.

The basic wing-with-interference data are presented as angle of attack, drag coefficient, and pitching-moment coefficient against lift coefficient in figure 7. The configurations designated A, B, C, and D indicate that bodies A, B, C, and D, respectively, in figures 7(a) to 7(f) were tested in conjunction with the wing. The data are shown first for the various wing-body configurations for angles of attack from 0° to 7° and then for configuration D for angles of attack from 0° to 28° .

Base-pressure coefficients are presented in figures 8(a) to 8(c) for the bodies, the wing-body combinations, and the incremental values due to addition of the wing to the bodies. For body D, base-pressure data were obtained through the low angle-of-attack range with the aluminum wing on the body and through the high angle-of-attack range with the steel wing on the body. The two sets of information are shown to indicate the repeatability of the data. All data presented have been

adjusted for model base drag, the coefficients having been adjusted to a condition at which the base pressure is equal to the stream static pressure, so that the results do not include drag due to the base of the model.

From these basic data, all the analysis figures numbered from 9 to 17 have been prepared.

In order to facilitate presentation of the data, staggered scales have been used in many figures and care should be taken in selecting the zero axis for each curve.

DISCUSSION

Bodies

The basic data for the original body and the various modifications investigated indicate that the most pronounced changes in the aerodynamic characteristics of the bodies occurred in the transonic speed range and the most interesting phenomenon was the effect of body shape on the drag rise.

Lift.- The total lift on bodies of the type investigated is small and from figures 6(a) and 9, there appear to be no radical changes with increasing Mach number at any angle of attack.

Drag.- The drag rise of the various bodies investigated began at a Mach number of the order of 1.00 and was essentially completed at a Mach number of 1.05, (fig. 10). The drag rise is defined as that increase in drag which occurs with the onset of shock formation and associated flow separation as Mach number is increased.

Local Mach number distributions on the original body at zero angle of attack, obtained from pressure measurements of reference 4, and schlieren surveys shown in reference 2 indicate that, starting at a subsonic stream Mach number of 0.98, the flow was supersonic over a relatively extensive region of the original body. The schlieren surveys also indicated that this region of supersonic flow extended well away from the body and extensive, nearly normal shock was associated with the adverse pressure gradients downstream of the supersonic-flow regions. The drag of the original body was associated primarily with these phenomena.

At zero angle of attack, when the forebody of the original body was extended and a cylindrical midsection inserted between the extended fore body and the original afterbody to form body B, the drag rise up to a Mach number of 1.05 was essentially the same, within the accuracy of

this test, as for the original body A (fig. 10). At high Mach numbers, the drag increase for body B is greater than for body A.

A sizable reduction in drag rise is shown for the body using the cylindrical afterbody in combination with the original forebody (body C). It is indicated that the use of this cylindrical afterbody decreased the magnitude and extent of the induced velocities over the rear portion of the body and thereby reduced or eliminated the drag-producing normal shock associated with the original afterbody. It may be assumed that the use of the cylindrical afterbody eliminated the effect of the original afterbody. Thus, the reduction in drag rise associated with the use of the cylindrical afterbody is an indication of the relative drag rise associated with the original afterbody. On the basis of a comparison of the results of the two cases, it is indicated that approximately 50 percent of the drag rise for bodies A and B in the transonic speed range can be charged directly to the shape of the original afterbody.

Figure 10 also indicates that within the order of accuracy of the test, the drag rise for bodies C and D is essentially the same. This might be expected since both bodies incorporated the cylindrical afterbody and were influenced by the same forebody pressures. The absolute drag for body D is shown to be greater than for body C at subsonic as well as supersonic speeds. This is directly associated with the greater wetted area of body D.

With increase in angle of attack up to 7° , the relation between bodies A, B, C, and D remained about the same as regards the drag rise in the transonic range. In figure 6(b), it is shown that at the higher angles of attack for body D, the increase in drag coefficient with angle of attack becomes more pronounced.

Pitching moments.— The modifications to the original body had definite effects on the pitching-moment characteristics for the angle-of-attack cases (fig. 11). The extended forebody produced pitching-moment coefficients considerably more positive than those for the original body. The use of the cylindrical afterbody resulted in a pitching-moment coefficient more negative than for the original body. This less positive pitching-moment coefficient is indicative of a possible positive loading, or at least a less negative loading, on the cylindrical afterbody than on the original afterbody. In reference 5, it was shown that, at low angles of attack, the positive pitching-moment coefficient of the original body was due in part to a negative load over the curved afterbody. The pitching-moment coefficient for the body with the extended forebody and cylindrical afterbody (body D) was essentially the same as for the original body. The effect of the extended forebody and the effect of the cylindrical afterbody canceled each other.

At angles of attack up to 7° , the pitching-moment coefficients of the various bodies investigated were generally only slightly affected by changes in Mach number. The variation of pitching-moment coefficient with angle of attack shown in figure 6(c) indicated that, with increase in angle of attack up to 28° , the changes in pitching moment for body D were gradual throughout the Mach number range of the test and no radical characteristics were indicated.

Wing With Interference

The induced flow field around a wing as for a body generally results in shock waves at transonic speeds. The energy losses in these shocks and the possible associated boundary-layer separation result in the drag rise for the configuration. The addition of the flow field of a wing to that of a body may result in stronger shocks and separation for the combination than those present for the individual components. These effects may alter the aerodynamic characteristics, especially the drag, of the combination. This section is concerned with the effect of the body-shape changes on this interference of the body on the wing characteristics.

The various body shapes were developed primarily to reduce the effects of interference between the wing and body. The forebody was extended in an attempt to reduce the induced velocities produced by the body in the region of the forward portion of the wing. The cylindrical afterbody was added in an attempt to reduce the induced velocities and adverse gradients produced by the original afterbody in the region of the rearward part of the wing (ref. 6).

Lift.- In figure 12, the lift-coefficient data at high angles of attack for the wing in the presence of body A (ref. 1) and similar data for the wing in the presence of body D show that the interference effect of a large change in body shape had only a small influence on the lift characteristics of the wing with interference up to the highest angle of attack tested. Data are included in figure 12 for the aluminum wing in the presence of body A (ref. 7) to indicate the close agreement and repeatability of test information in the Langley 8-foot transonic tunnel.

In figure 13 are presented the effects of interference from the four bodies (A, B, C, and D) on the average lift-curve slope of the wing with interference for the angle-of-attack range from 0° to 7° . In general, it appears that interference associated with the various body modifications produced only a slight increase in lift-curve slope for the wing with interference over the angle of attack and Mach number range tested. A consideration of these moderate effects should not lead to significant changes in the design of an airplane.

Drag.- The effects of wing-body interference on the drag characteristics of the wing are presented in terms of drag coefficient with Mach number for lift coefficients of 0, 0.2, and 0.4 in figure 14. The effects are shown to be most pronounced in the transonic range as was the case for the bodies alone.

Induced velocities over the wing-body combination lead to an earlier, stronger bow shock ahead of the leading edge of the wing-body juncture than would be expected ahead of the leading edge of the wing alone. It was reasoned that by extending the forebody the induced velocities in the region of the leading edge of the wing-body juncture would be reduced to such an extent that a sizable reduction in interference drag associated with the bow shock would result. The results presented in figure 14 for a lift coefficient of 0 indicate that extension of the forebody forward 2 diameters resulted in only a small change in the drag of the wing with interference at transonic Mach numbers between 0.975 and 1.05. Either the extension did not produce a reduction in induced velocities over the wing of sufficient magnitude to reduce the interference effect or the interference effect produced by these induced velocities was small.

The existence of a nearly normal shock perpendicular to the plane of symmetry and behind the trailing edge of the wing-body combination has been observed (ref. 6). Such a shock is also known from unpublished results to exist for a swept wing alone. The induced flow produced by the curved afterbody results in higher induced velocities ahead of the wing shock compared to those associated with the wing alone. As a result, the shock losses are probably increased by the presence of the body. In this case, it was reasoned that the use of a cylindrical afterbody would reduce the induced velocities and reduce the strong shock and associated interference drag of the original afterbody. The reduction of the extensive induced velocities over the cylindrical afterbody and the presence of considerably weaker shocks in the field of the combination may be attributed basically to less rapid rates of change of the cross-sectional areas for the combination employing the cylindrical afterbody compared to those for the curved original afterbody. See reference 8. It is shown in figure 14 that the use of a cylindrical afterbody in place of the original afterbody resulted in a marked reduction in the wing-with-interference drag at transonic Mach numbers. This improvement resulted in a 50-percent reduction in drag rise at a Mach number of 1.00.

At a lift coefficient of 0.4, the extended forebody played a more important role in producing a favorable interference effect at transonic speeds than did the cylindrical afterbody. The cylindrical afterbody was still effective in reducing the interference drag at transonic speeds; however, this reduction was not much greater than the reduction for the nonlifting case. The use of the extended forebody in combination

with the original afterbody (body B) indicated a reduction in drag rise of 40 percent at transonic speeds, whereas this extension resulted in only a 20-percent decrease in drag rise at zero lift.

A reduction of the induced velocities in the vicinity of the forward portion of the wing is more effective in reducing the drag rise for the lifting cases than for the nonlifting case at transonic speeds because the shocks that produce the drag for the lifting case are farther forward than those for the nonlifting case. These shocks would be measurably diminished by the reduced induced velocities in the forward region of the wing.

The decreases in drag coefficient for the lifting conditions lead to increases in the lift-to-drag ratio at transonic speeds. These increases are shown in figure 15 for the maximum lift-to-drag ratio. The maximum lift-drag ratios were favorably influenced at transonic speeds by each of the modifications to the original body. The $(L/D)_{\max}$ was about 11.4 for bodies B and C at a Mach number of 1.00 compared to 9.5 for body A. The effect of the two modifications used for bodies B and C, when combined, appeared to be additive. As a result, the value of the final configuration (body D) was 12.8 which is 35 percent greater than for the original configuration. This favorable effect decreased with increase in Mach number.

The lift coefficient at which $(L/D)_{\max}$ was obtained varied only slightly for the different body changes. As Mach number increased from 0.60 to 1.13, the average lift coefficient increased from about 0.19 to 0.25 with the greatest change occurring between Mach numbers of 0.95 and 1.00.

The maximum lift-drag ratio is also presented in figure 16 for the various modifications with an additional drag coefficient of 0.01 added to the experimental results. The additional value of drag coefficient of 0.01 is on the order of that which might be expected if a fuselage, canopy, empennage, and other protuberances were placed on the wing to form a real configuration. Thus, values of adjusted $(L/D)_{\max}$ are obtained at the higher lift coefficients (fig. 16) at which real airplanes would fly to obtain $(L/D)_{\max}$. Figure 16 indicates improvements in $(L/D)_{\max}$ can be expected in the transonic range for any of the modifications tested. The values of lift coefficient for which the adjusted maximum lift-drag ratio was obtained were approximately the same at a given Mach number for the various configurations investigated.

Pitching moment.- At lift coefficients up to 0.4, figure 17 indicates that the interference effects for the various body shapes on the pitching-moment coefficient of the wing were most pronounced through the transonic range. Even here the effects were moderate and tended only to make the values slightly more positive.

Investigations of many sweptback-wing—body combinations have demonstrated instability occurring at high and even moderate lift coefficients for those combinations which might otherwise present attractive performance characteristics. The steel wing in combination with body D was used in the present investigation primarily to obtain data at high angles of attack to determine the effect of a large change in body shape on the pitch-up characteristics of the wing. In figure 7(f), pitching-moment coefficients for the steel wing in the presence of body D are compared with pitching-moment coefficients for the same wing in the presence of body A (ref. 1). This comparison indicates that the large change in body shape from the original curved body A to body D, with its extended forebody and cylindrical afterbody, did not cause any significant difference in the pitch-up characteristics of the wing with interference. The magnitude of pitch-up and variation with Mach number were approximately the same. The lift coefficient at which pitch-up occurred for both configurations was of the order of 0.6. In general, the only effect of the large body change on the moments, for lift coefficients up to and through pitch-up, was an indication of slightly more positive moments for the wing in the presence of body D.

CONCLUSIONS

The investigation of a 45° sweptback wing in combination with a systematic series of body shapes and the bodies alone has led to the following conclusions:

1. The principal effects of changes in body shape on the interference of the wing and body occurred in the transonic speed range.
2. The drag of the wing with interference was most significantly affected by the various body changes. The interference effect of the various body modifications on the lift and pitching moment of the wing up to the highest angles of attack tested was small and should not affect the design of an aircraft. The pitch-up characteristics of the sweptback wing were relatively unaffected by the largest body modification investigated.
3. The zero-lift drag rise of the wing with interference associated with the curved original afterbody was reduced 50 percent by the use of the cylindrical afterbody in combination with the wing at a Mach number of approximately 1.00.
4. The maximum lift-drag ratio of the wing with interference in combination with the original body was improved 35 percent in the transonic range by extending the forebody and adding a cylindrical section from the vicinity of the leading edge of the wing-body juncture rearward to the base of the model.

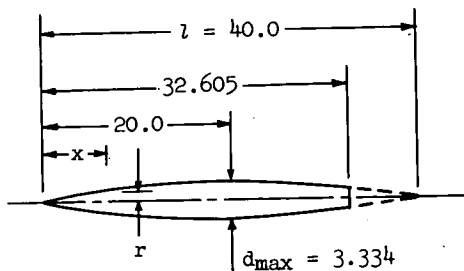
5. The changes in body shape had significant effects on the drag characteristics of the bodies alone at transonic speeds and on the pitching-moment characteristics throughout the speed range of the investigation.

Langley Aeronautical Laboratory,
National Advisory Committee for Aeronautics,
Langley Field, Va.

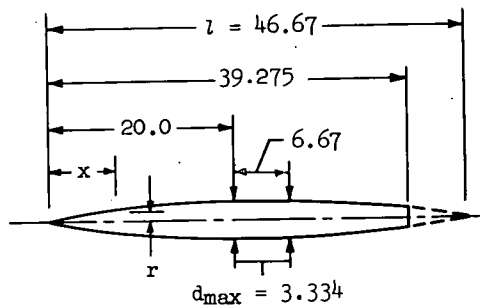
REFERENCES

1. Osborne, Robert S., and Mugler, John P., Jr.: Aerodynamic Characteristics of a 45° Sweptback Wing-Fuselage Combination and the Fuselage Alone Obtained in the Langley 8-Foot Transonic Tunnel. NACA RM L52E14, 1952.
2. Ritchie, Virgil S., and Pearson, Albin O.: Calibration of the Slotted Test Section of the Langley 8-Foot Transonic Tunnel and Preliminary Experimental Investigation of Boundary-Reflected Disturbances. NACA RM L51K14, 1952.
3. Osborne, Robert S.: A Transonic-Wing Investigation in the Langley 8-Foot High-Speed Tunnel at High Subsonic Mach Numbers and at a Mach Number of 1.2. Wing-Fuselage Configuration Having a Wing of 45° Sweepback, Aspect Ratio 4, Taper Ratio 0.6, and NACA 65A006 Airfoil Section. NACA RM L50H08, 1950.
4. Loving, Donald L., and Williams, Claude V.: Basic Pressure Measurements on a Fuselage and a 45° Sweptback Wing-Fuselage Combination at Transonic Speeds in the Slotted Test Section of the Langley 8-Foot High-Speed Tunnel. NACA RM L51F05, 1951.
5. Estabrooks, Bruce B.: An Analysis of the Pressure Distribution Measured on a Body of Revolution at Transonic Speeds in the Slotted Test Section of the Langley 8-Foot Transonic Tunnel. NACA RM L52D21a, 1952.
6. Whitcomb, Richard T., and Kelly, Thomas C.: A Study of the Flow Over a 45° Sweptback Wing-Fuselage Combination at Transonic Mach Numbers. NACA RM L52D01, 1952.
7. Osborne, Robert S., and Mugler, John P., Jr.: Effects of Wing Elasticity on the Aerodynamic Characteristics of a 45° Sweptback-Wing-Fuselage Combination Measured in the Langley 8-Foot Transonic Tunnel. NACA RM L52G23, 1952.
8. Whitcomb, Richard T.: A Study of the Zero-Lift Drag-Rise Characteristics of Wing-Body Combinations Near the Speed of Sound. NACA RM L52H08, 1952.

TABLE I
ORDINATES AND DIMENSIONS OF BODIES A AND B



Body A

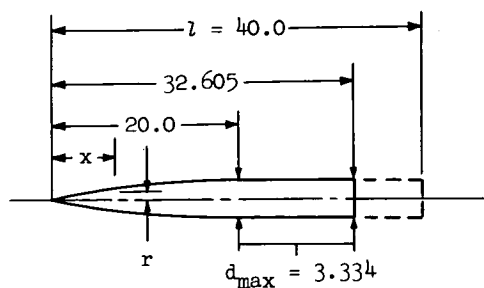


Body B

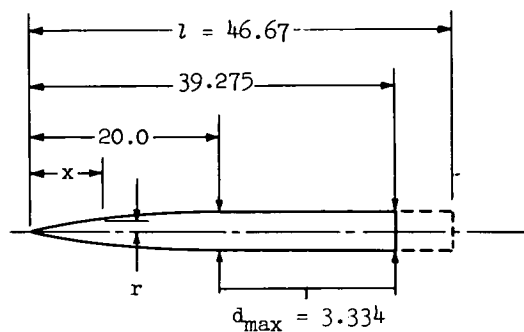
Fuselage ordinates	
x/l	r/l
0	0
.0050	.00231
.0075	.00298
.0125	.00428
.0250	.00722
.0500	.01205
.0750	.01613
.1000	.01971
.1500	.02593
.2000	.03090
.2500	.03465
.3000	.03741
.3500	.03933
.4000	.04063
.4500	.04143
.5000	.04167
.5500	.04130
.6000	.04024
.6500	.03842
.7000	.03562
.7500	.03128
.8000	.02526
.8333	.02083
.8500	.01852
.9000	.01125
.9500	.00439
1.0000	0
L.E. radius = 0.0005	

Fuselage ordinates	
x/l	r/l
0	0
.0043	.00198
.0064	.00255
.0107	.00367
.0214	.00619
.0429	.01033
.0643	.01382
.0857	.01689
.1286	.02222
.1714	.02648
.2143	.02970
.2571	.03206
.3000	.03371
.3428	.03482
.3857	.03551
.4285	.03571
.4750	.03571
.5000	.03571
.5250	.03571
.5500	.03571
.5715	.03571
.6144	.03539
.6572	.03449
.7000	.03293
.7429	.03053
.7858	.02681
.8286	.02165
.8571	.01734
.8714	.01587
.9143	.00964
.9571	.00376
1.0000	0
L.E. radius = 0.0005	

TABLE II
ORDINATES AND DIMENSIONS OF BODIES C AND D



Body C



Body D

Fuselage ordinates	
x/l	r/l
0	0
.0050	.00231
.0075	.00298
.0125	.00428
.0250	.00722
.0500	.01205
.0750	.01613
.1000	.01971
.1500	.02593
.2000	.03090
.2500	.03465
.3000	.03741
.3500	.03933
.4000	.04063
.4500	.04143
.5000	.04167
.5500	.04167
.6000	.04167
.6500	.04167
.7000	.04167
.7500	.04167
.8000	.04167
.8333	.04167
.8500	.04167
.9000	.04167
.9500	.04167
1.0000	.04167
L.E. radius = 0.0005	

Fuselage ordinates	
x/l	r/l
0	0
.0043	.00198
.0064	.00255
.0107	.00367
.0214	.00619
.0429	.01033
.0643	.01382
.0857	.01689
.1286	.02222
.1714	.02648
.2143	.02970
.2571	.03206
.3000	.03371
.3428	.03482
.3857	.03551
.4285	.03571
.4750	.03571
.5000	.03571
.5250	.03571
.5500	.03571
.5715	.03571
.6144	.03571
.6572	.03571
.7000	.03571
.7429	.03571
.7858	.03571
.8286	.03571
.8571	.03571
.8714	.03571
.9143	.03571
.9571	.03571
1.0000	.03571
L.E. radius = 0.0005	

TABLE III
ACCURACY OF STRAIN-GAGE MEASUREMENTS

Aluminum wing data and body alone data, $\alpha = 0^\circ$ to 7° :

	<u>M = 0.60</u>	<u>M = 1.00</u>
C_L	± 0.008	± 0.004
C_D	± 0.001	± 0.0005
C_m	± 0.005	± 0.003

Steel-wing data, $\alpha = 0^\circ$:

	<u>M = 0.60</u>	<u>M = 1.00</u>
C_L	± 0.016	± 0.008
C_D	± 0.002	± 0.001
C_m	± 0.003	± 0.002

Steel-wing data, $\alpha = 28^\circ$:

	<u>M = 0.60</u>	<u>M = 1.00</u>
C_L	± 0.016	± 0.008
C_D	± 0.009	± 0.005
C_m	± 0.003	± 0.002



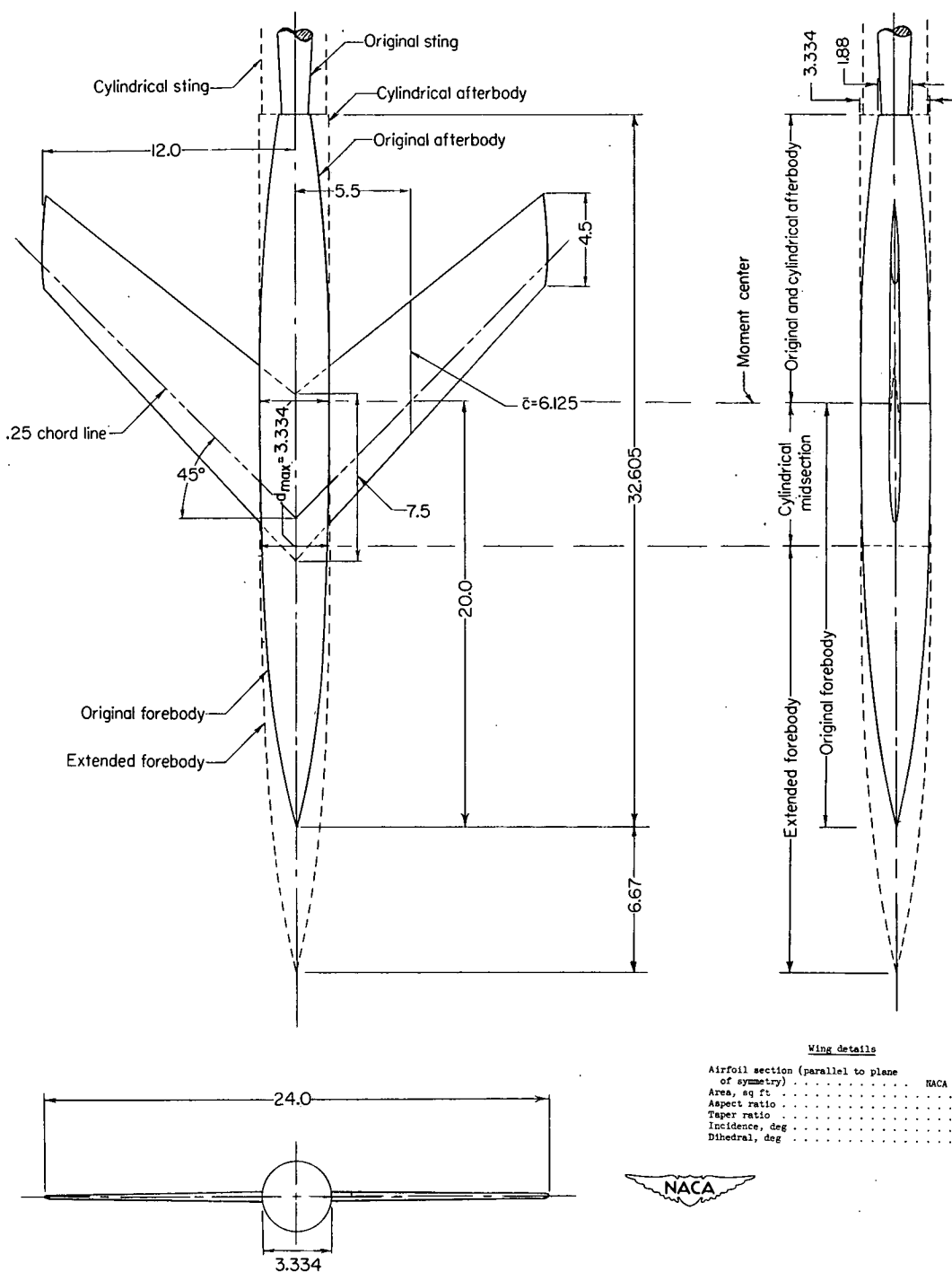
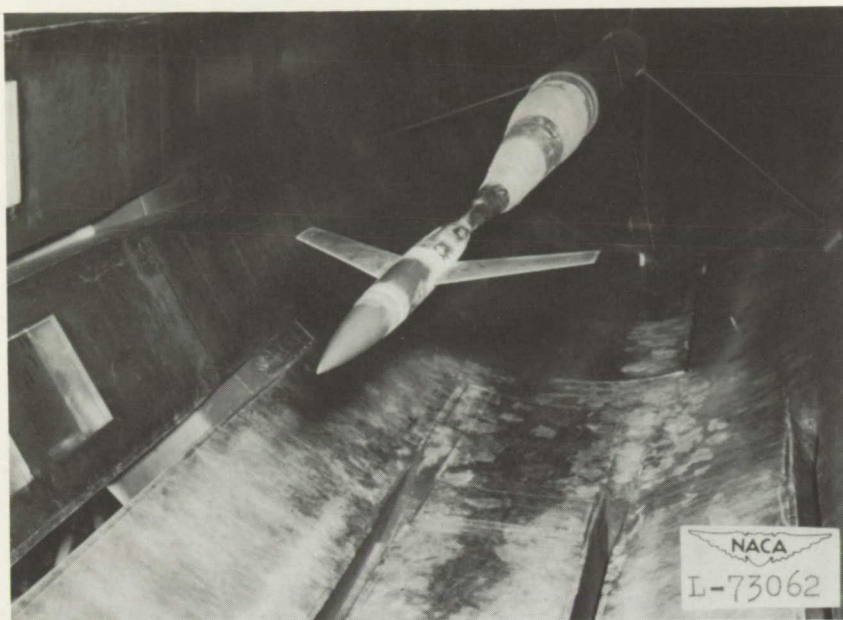


Figure 1.- Details of the wing-fuselage combination investigated in the slotted test section of the Langley 8-foot transonic tunnel. All dimensions are in inches.

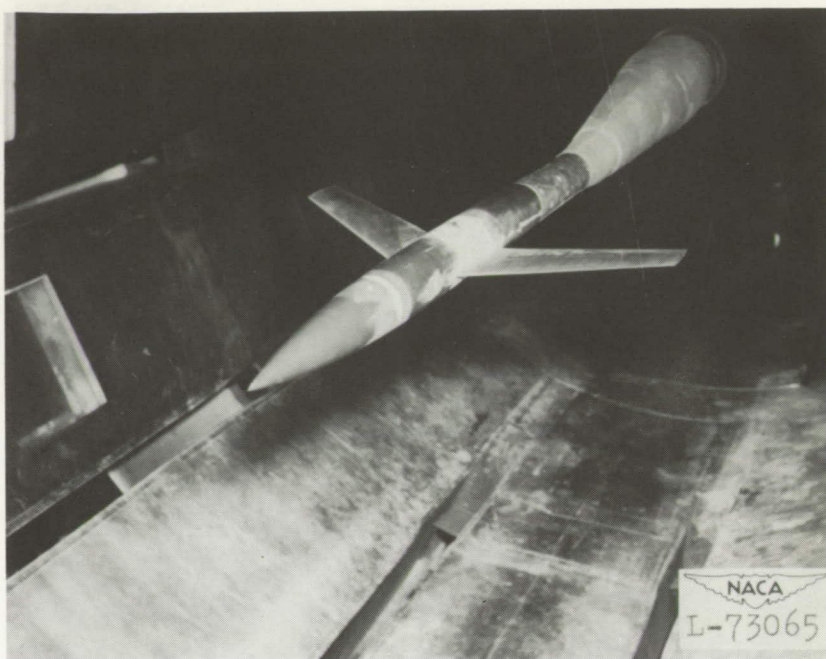


(a) Front view.

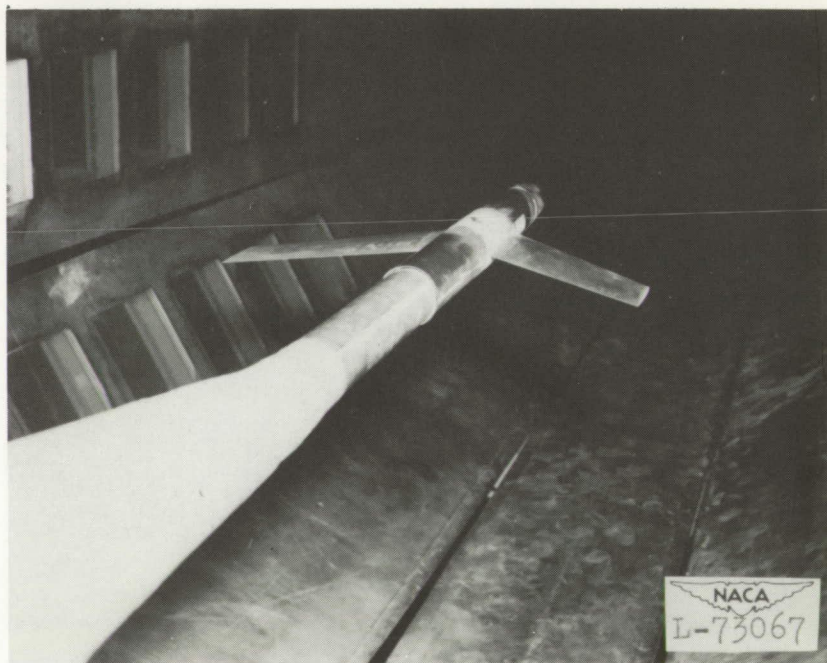


(b) Rear view.

Figure 2.- Wing-body combination with extended forebody and original afterbody (body B) in Langley 8-foot transonic tunnel.



(a) Front view.



(b) Rear view.

Figure 3.- Wing-body combination with extended forebody and cylindrical afterbody (body D) in Langley 8-foot transonic tunnel.

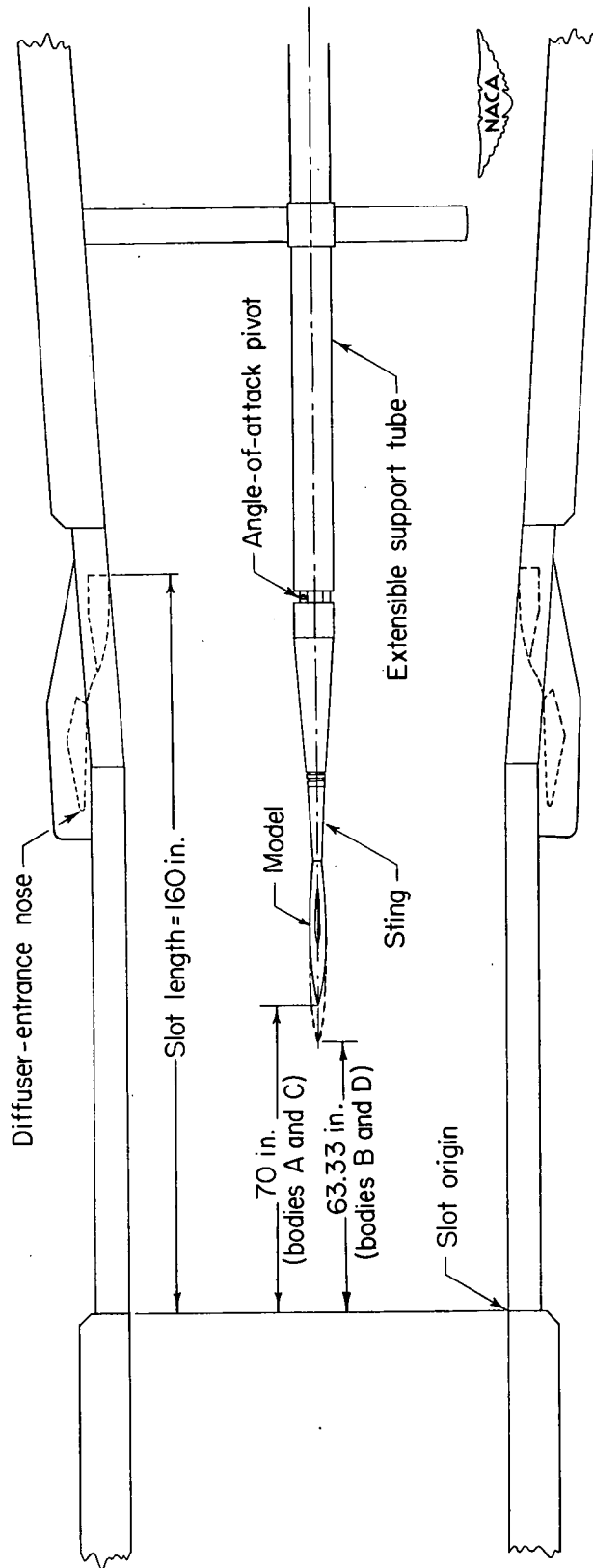


Figure 4.- Details of the location of the model in the slotted test section of the Langley 8-foot transonic tunnel.

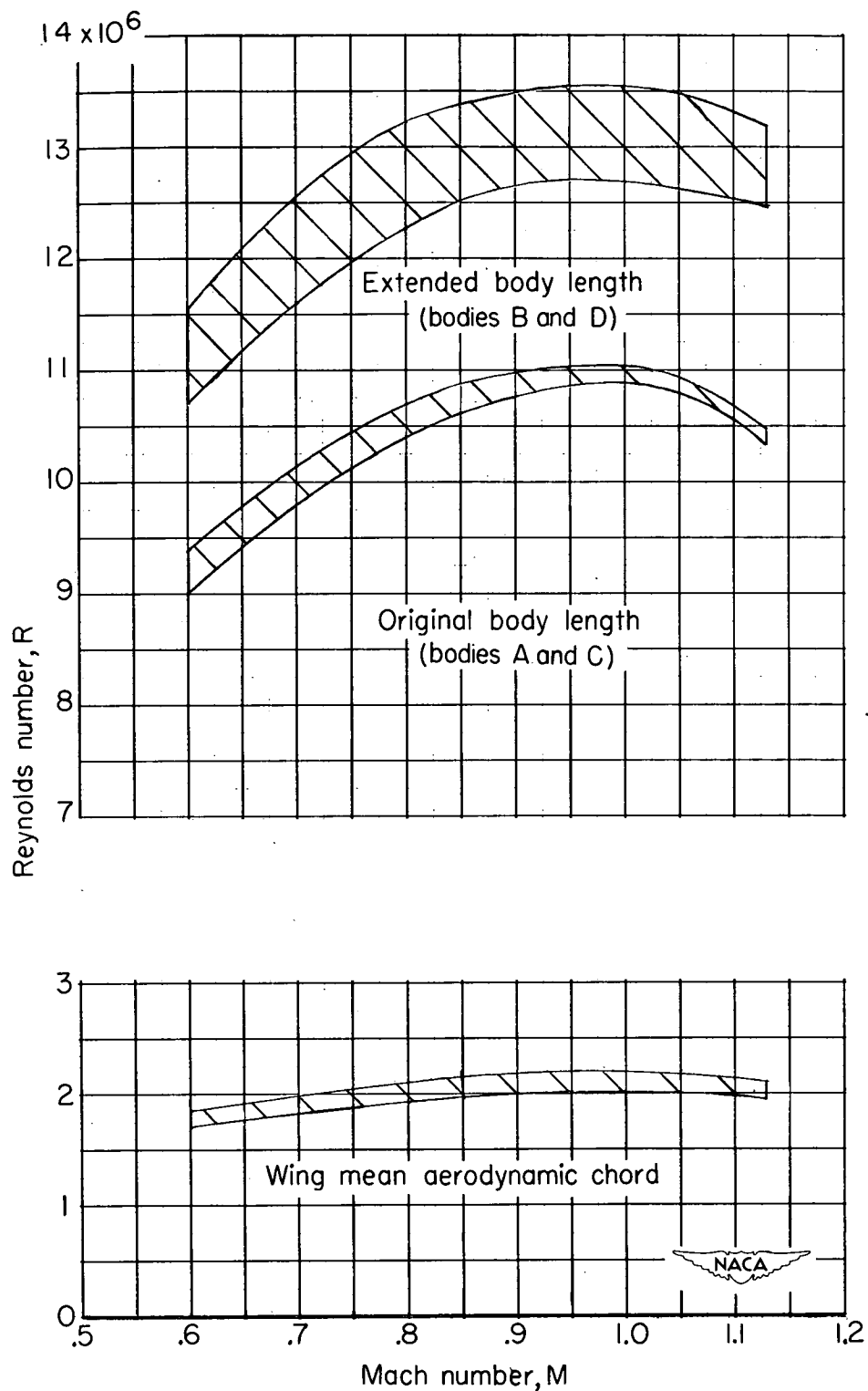
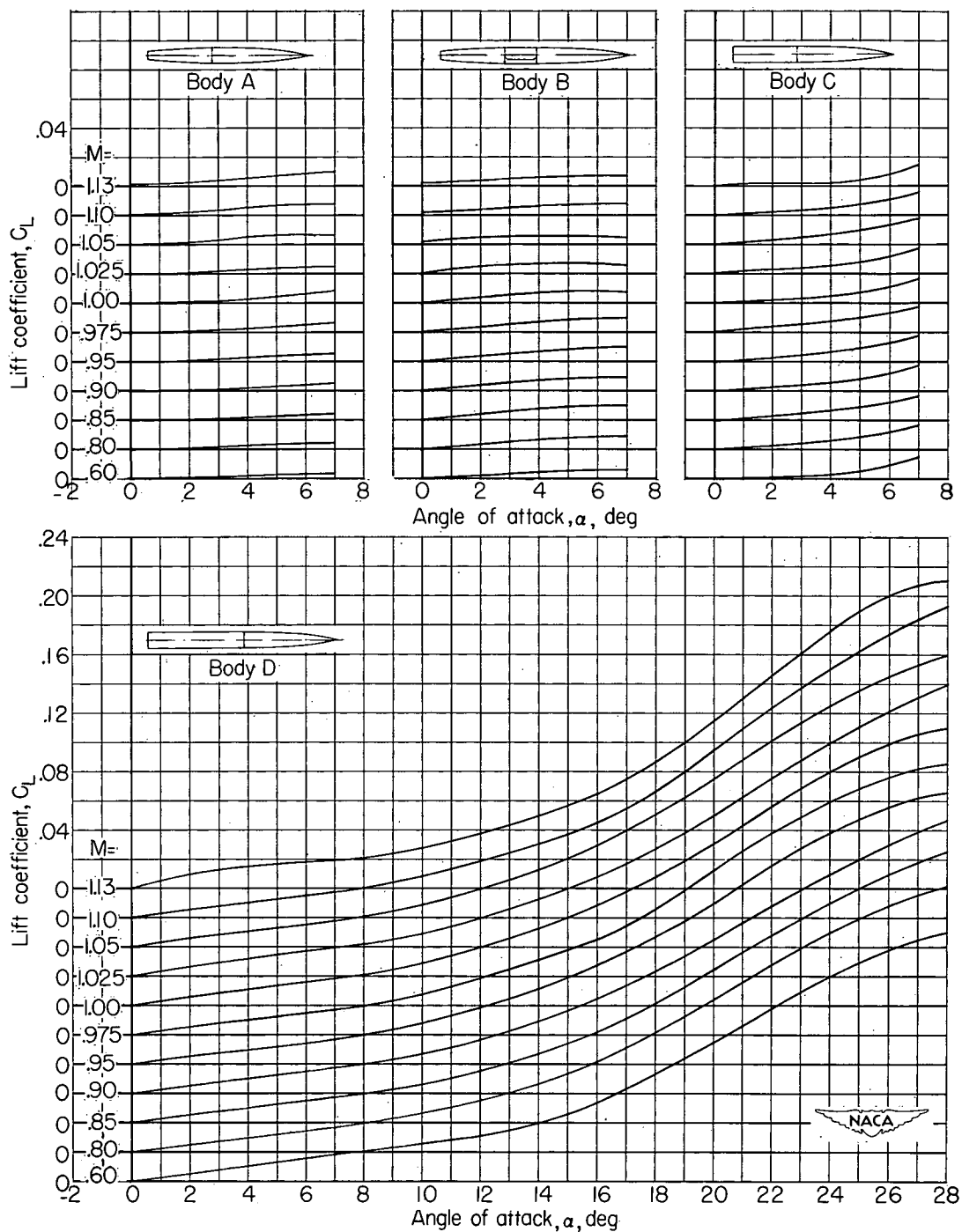
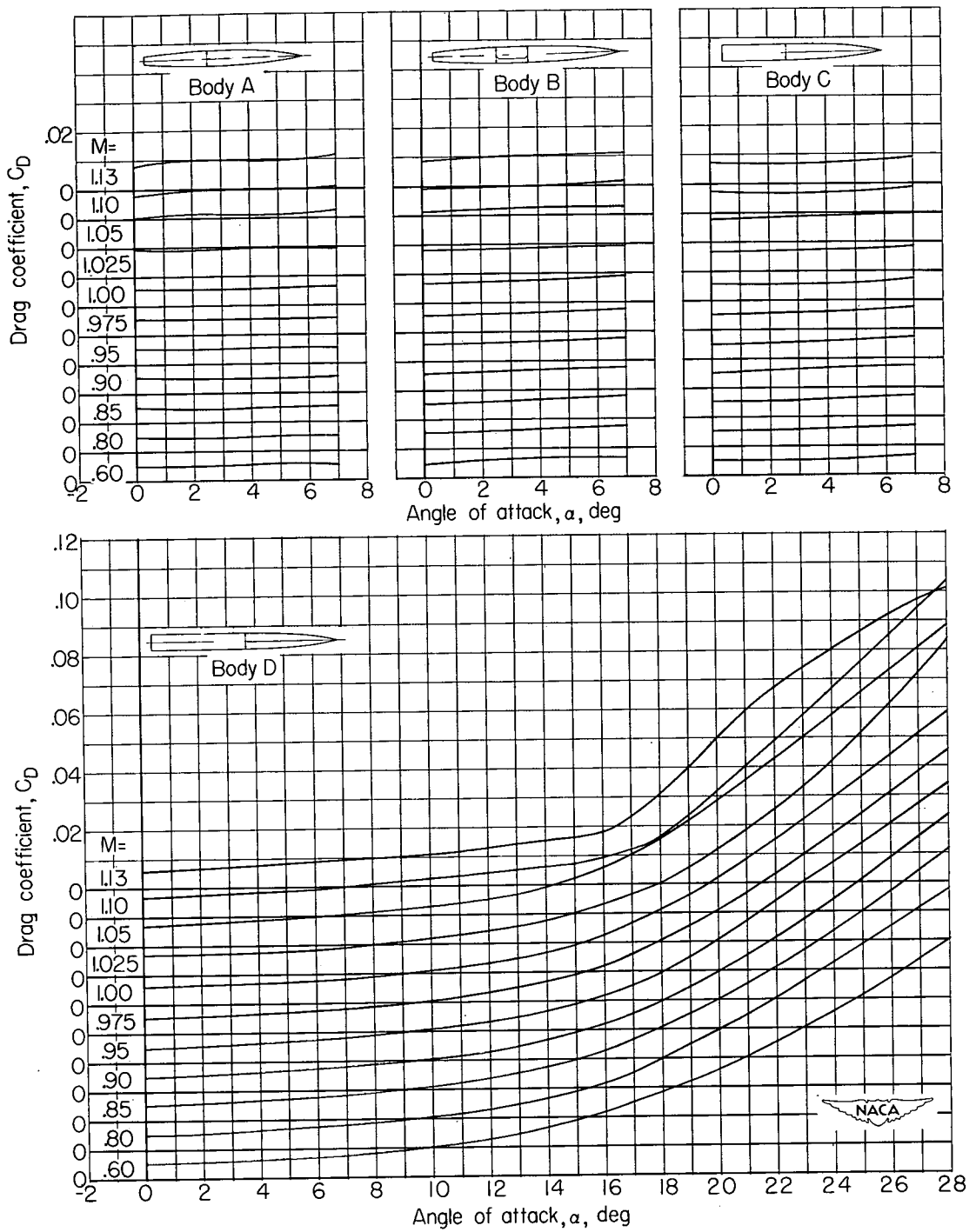


Figure 5.- Variation with Mach number of test Reynolds number based on body lengths and wing mean aerodynamic chord.



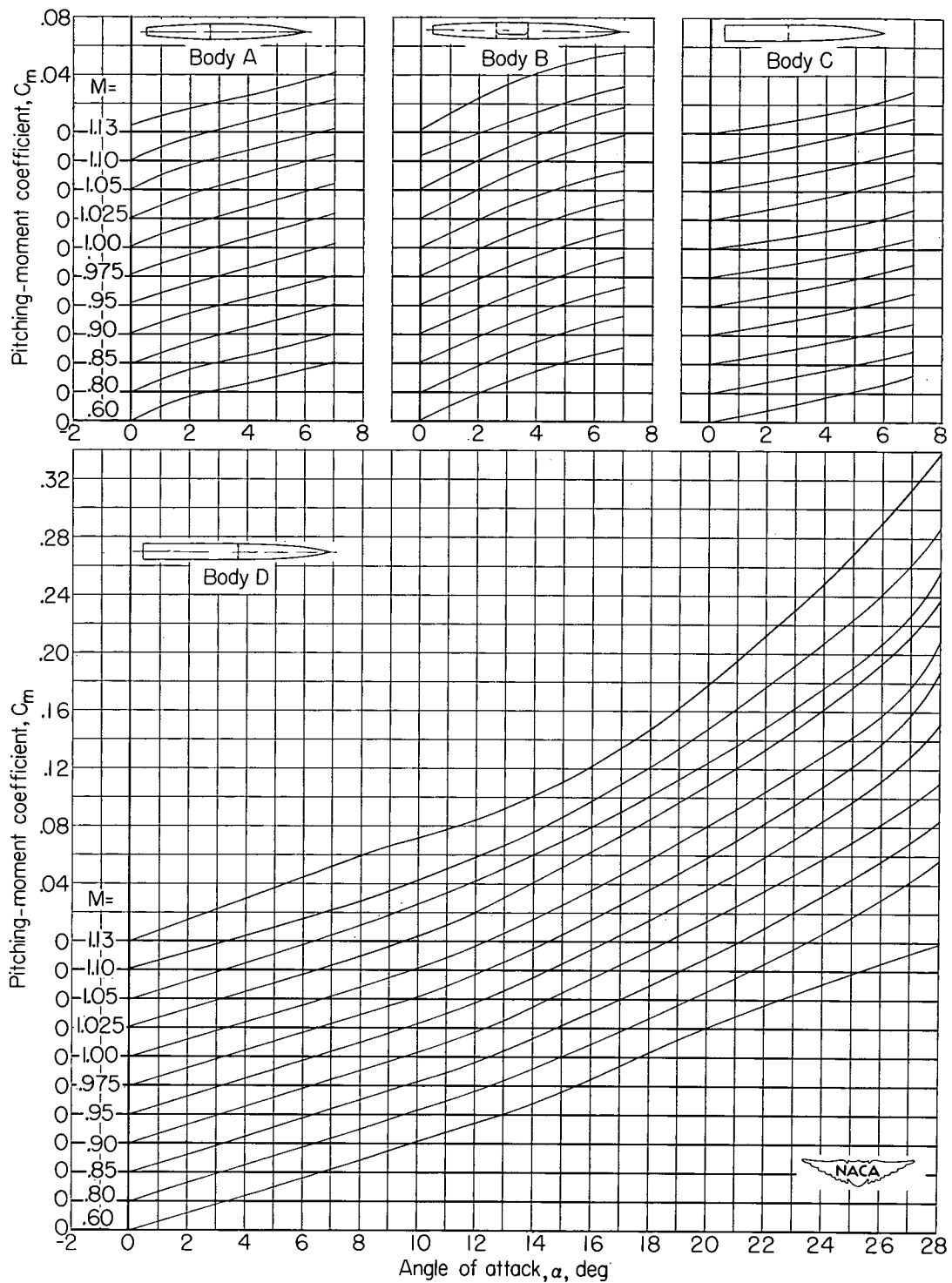
(a) Lift coefficient.

Figure 6.- Variation with angle of attack of the aerodynamic characteristics of the various bodies.



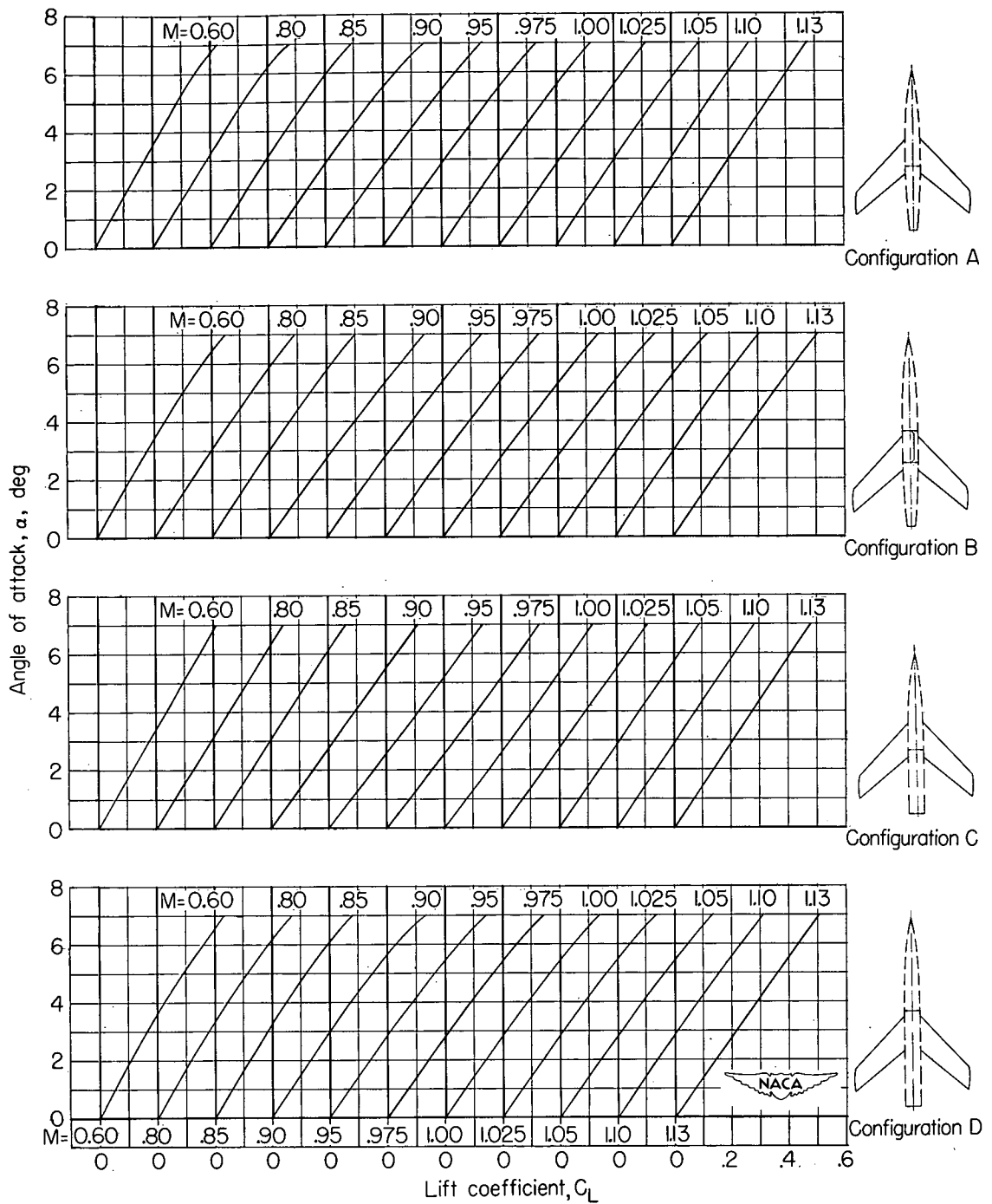
(b) Drag coefficient.

Figure 6.- Continued.



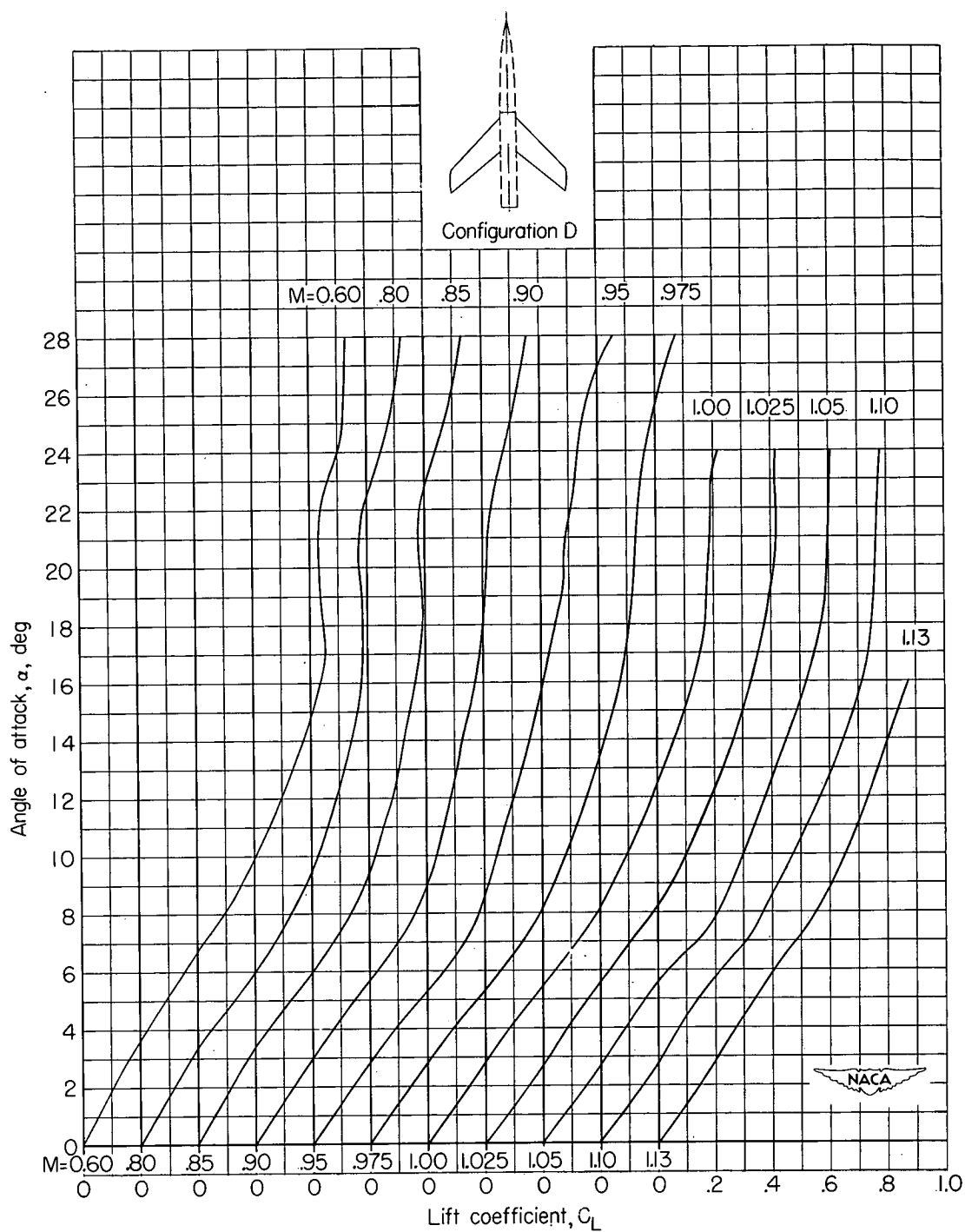
(c) Pitching-moment coefficient.

Figure 6.- Concluded.



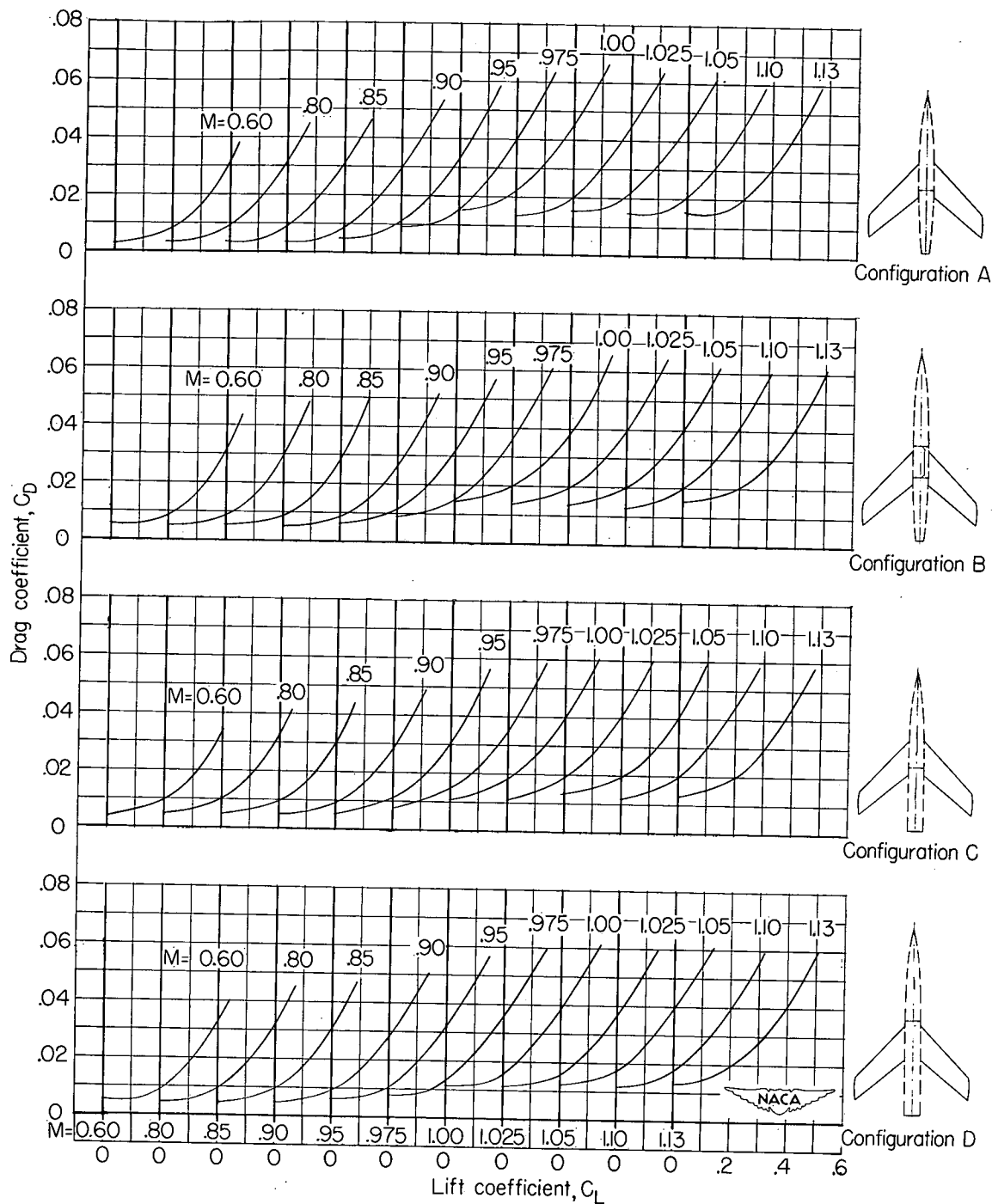
(a) Angle of attack; aluminum wing.

Figure 7.- Variation with lift coefficient of the aerodynamic characteristics of the aluminum and steel wings with interference for the various wing-body combinations.



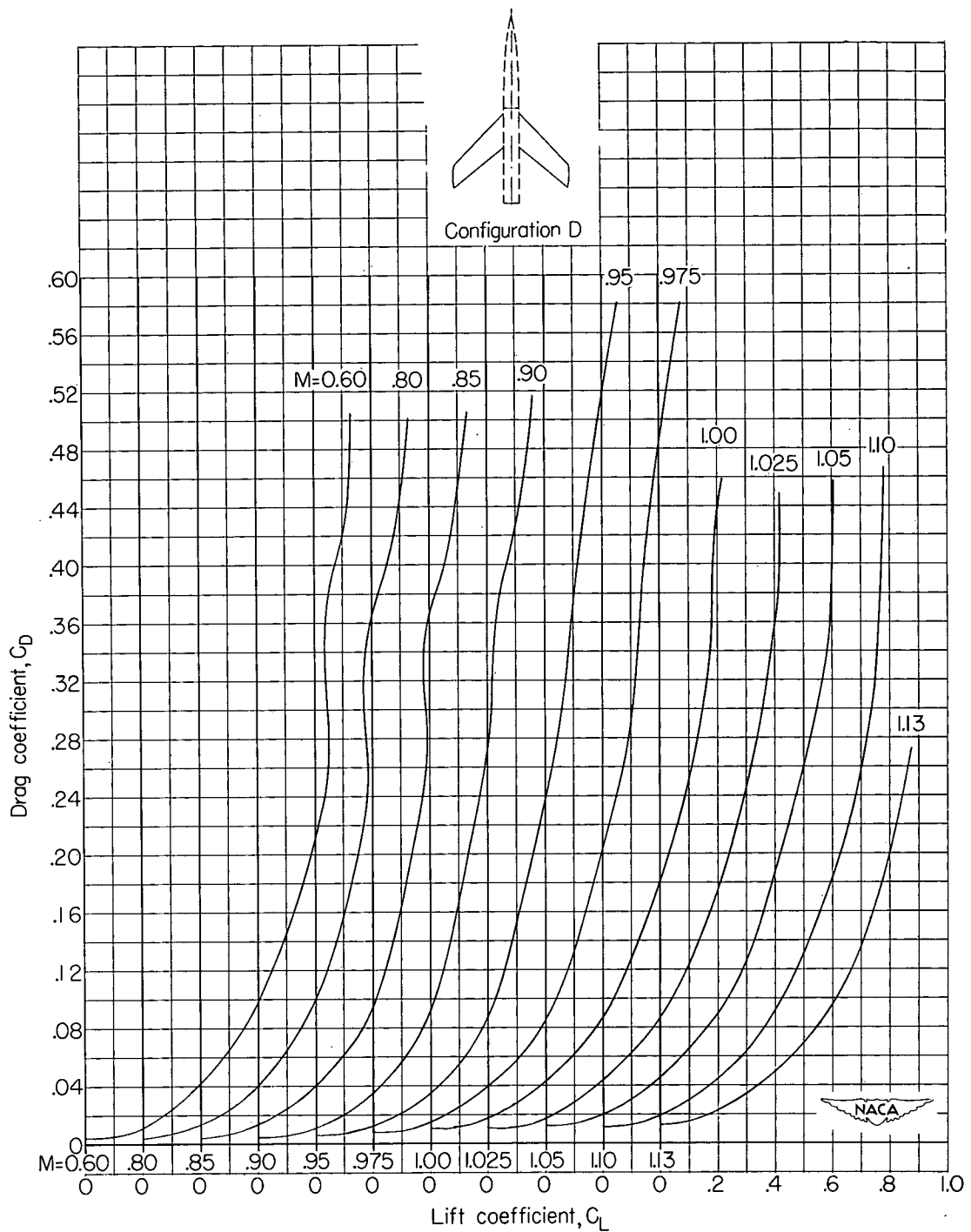
(b) Angle of attack; steel wing.

Figure 7.- Continued.



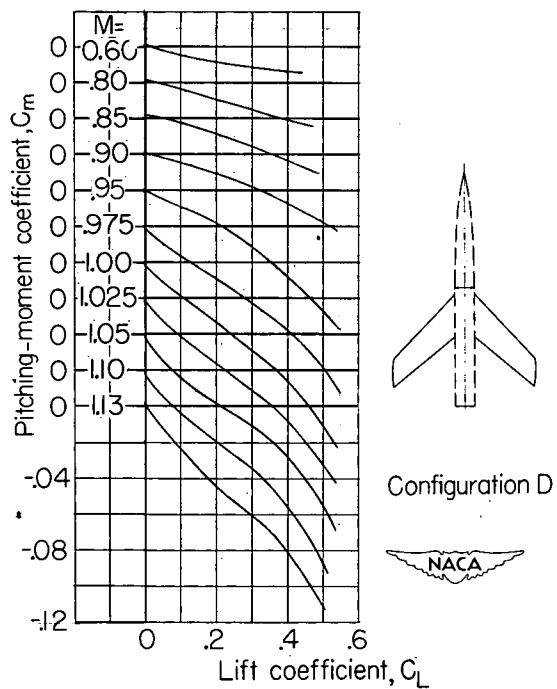
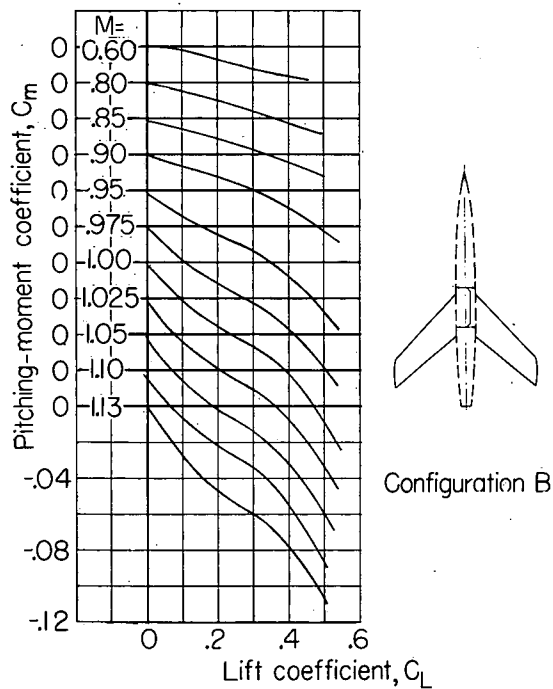
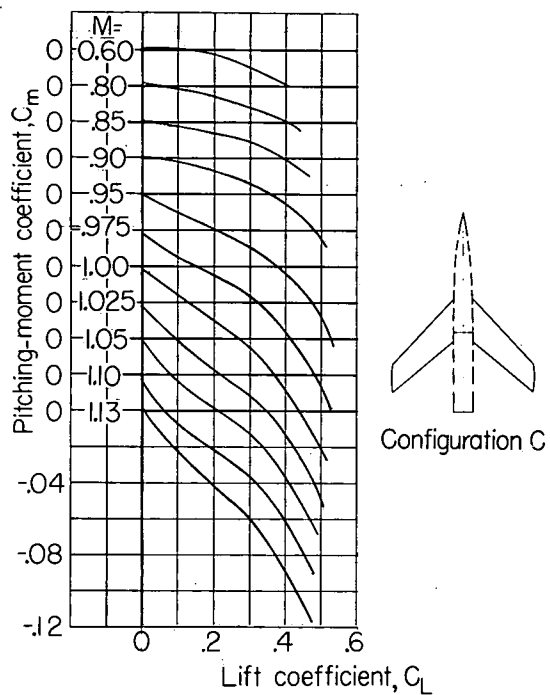
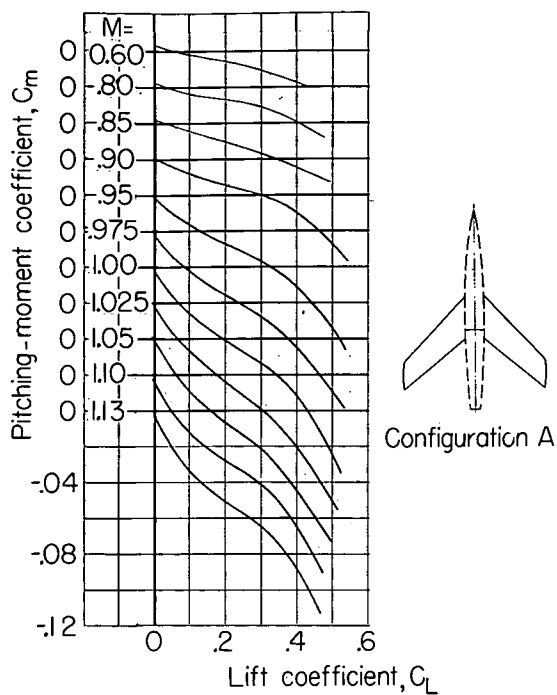
(c) Drag coefficient; aluminum wing.

Figure 7.- Continued.



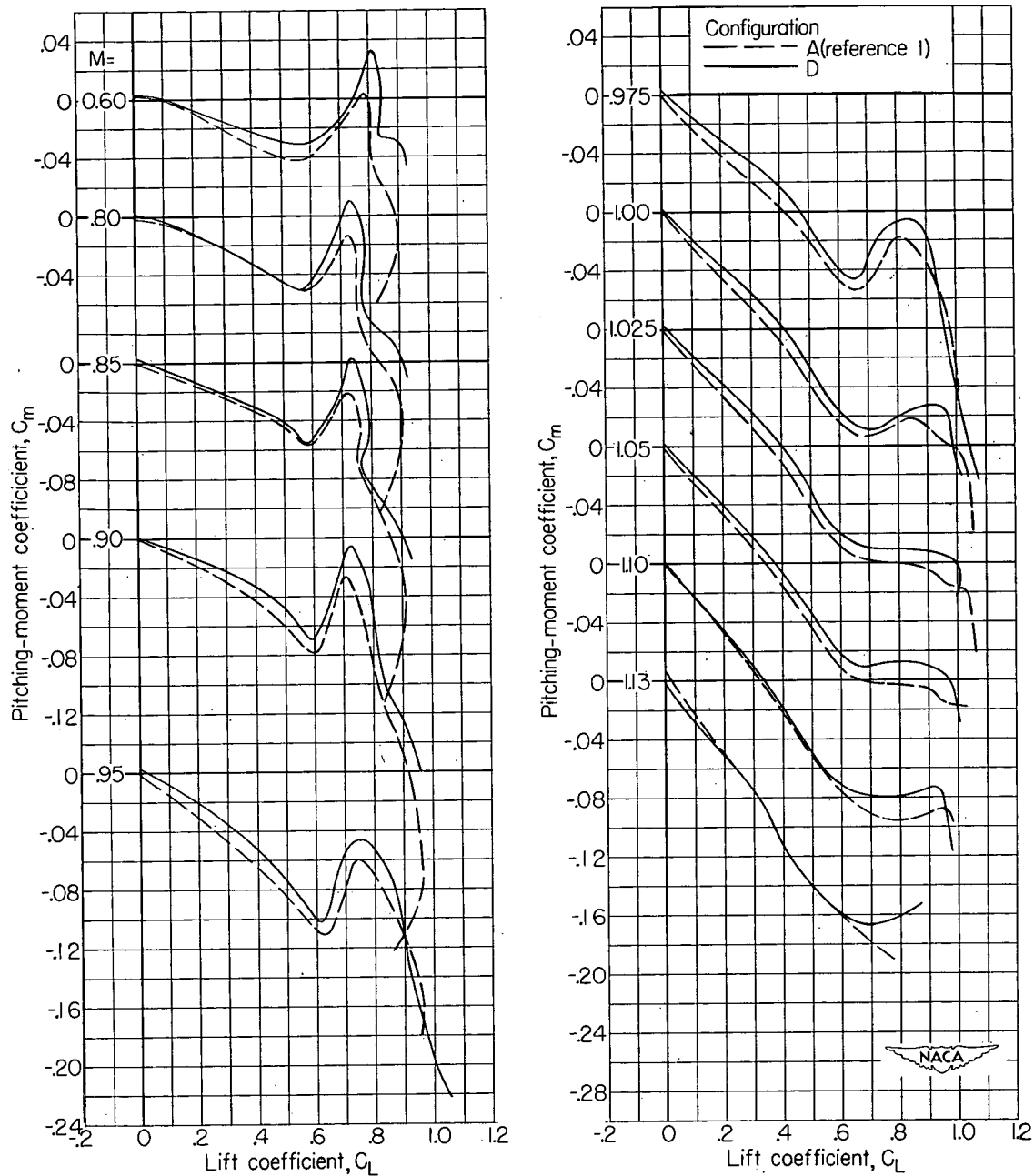
(d) Drag coefficient; steel wing.

Figure 7.- Continued.



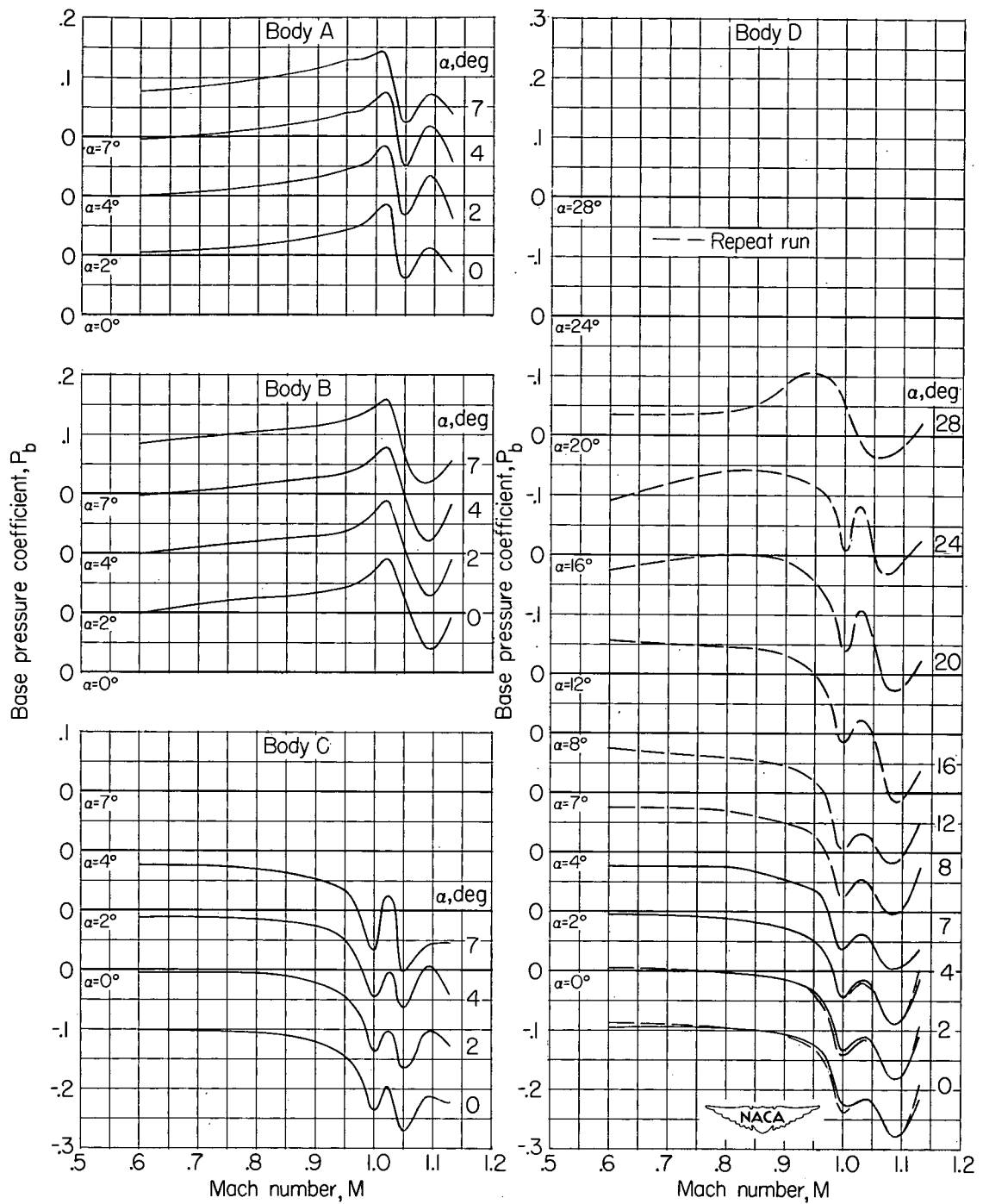
(e) Pitching-moment coefficient; aluminum wing.

Figure 7.- Continued.



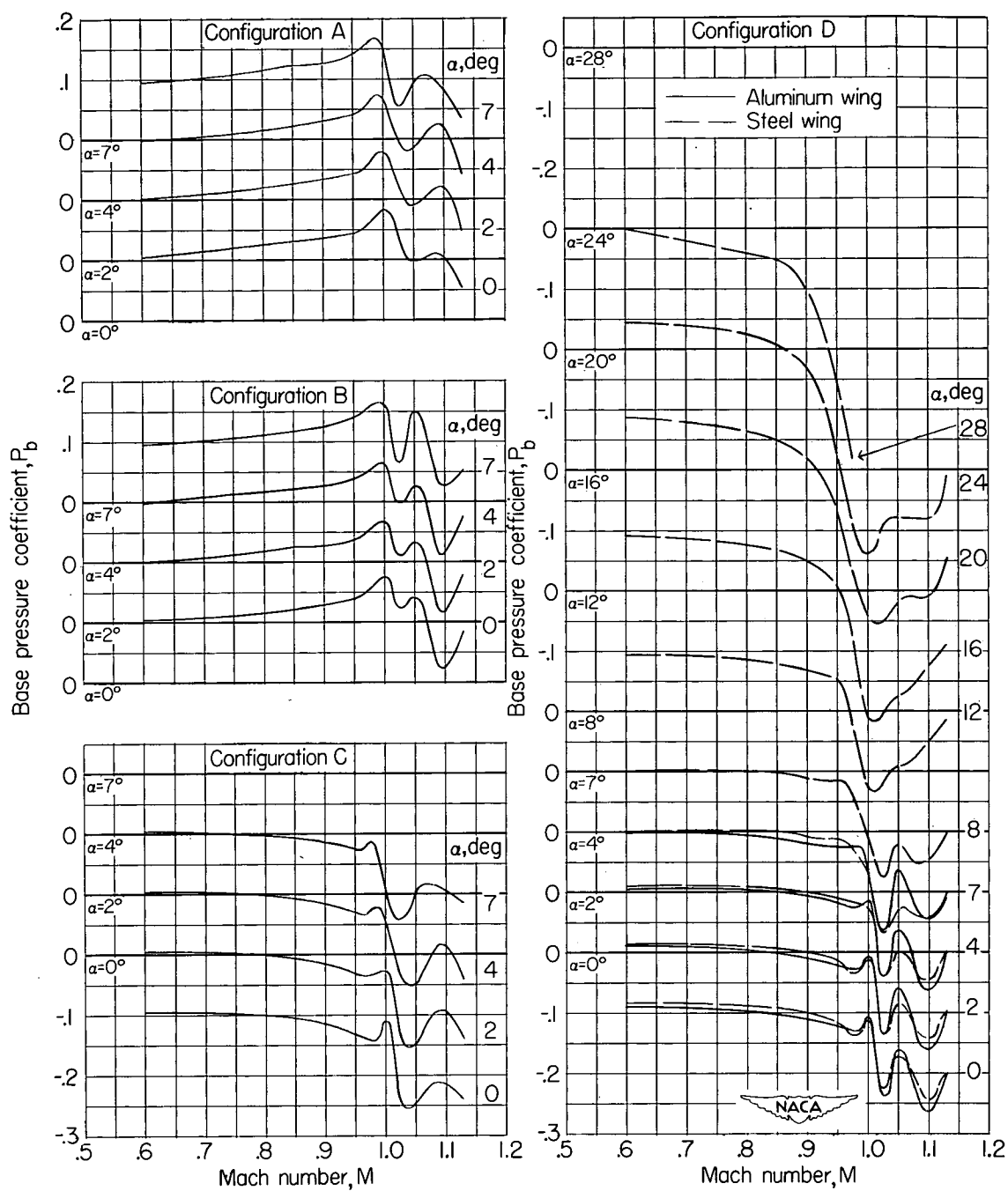
(f) Pitching-moment coefficient; steel wing.

Figure 7.- Concluded.



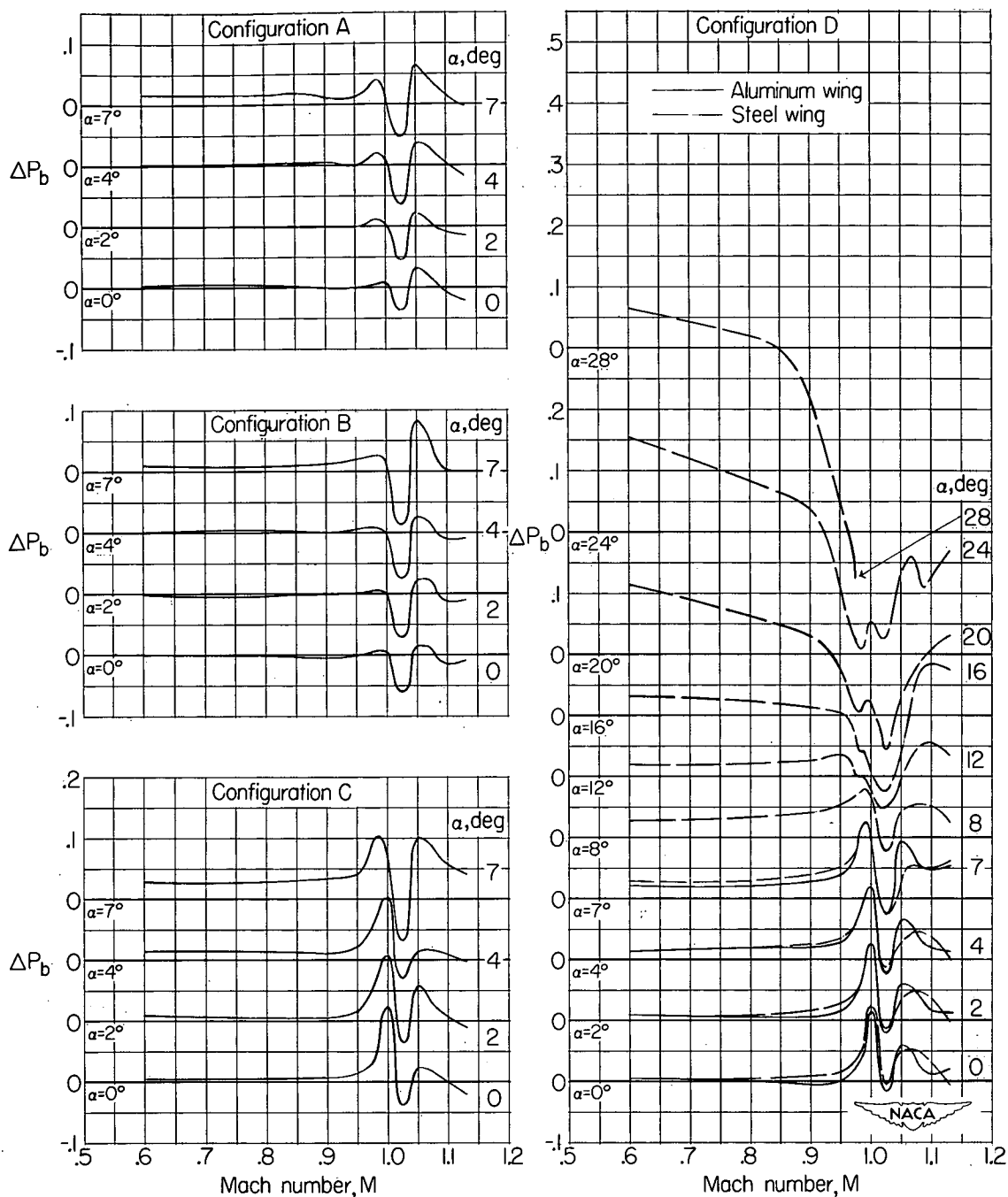
(a) Bodies.

Figure 8.- Variation with Mach number of the base-pressure coefficient for the various configurations investigated.



(b) Wing-body combinations.

Figure 8.- Continued.



(c) Wing influence on the base pressure coefficient of the various wing-body combinations.

Figure 8.- Concluded.

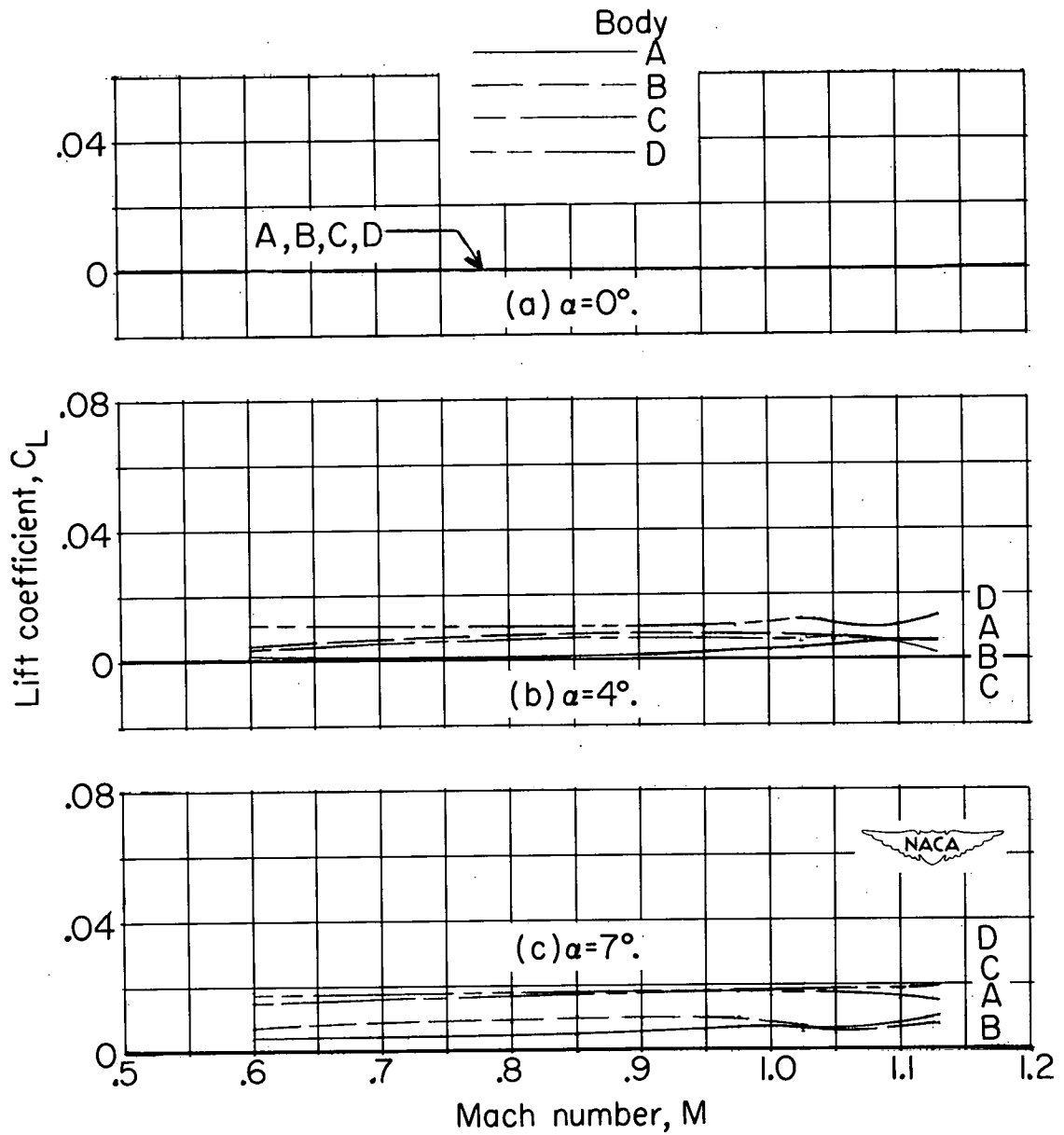


Figure 9.- Variation with Mach number of the lift coefficient of the various bodies at several angles of attack.

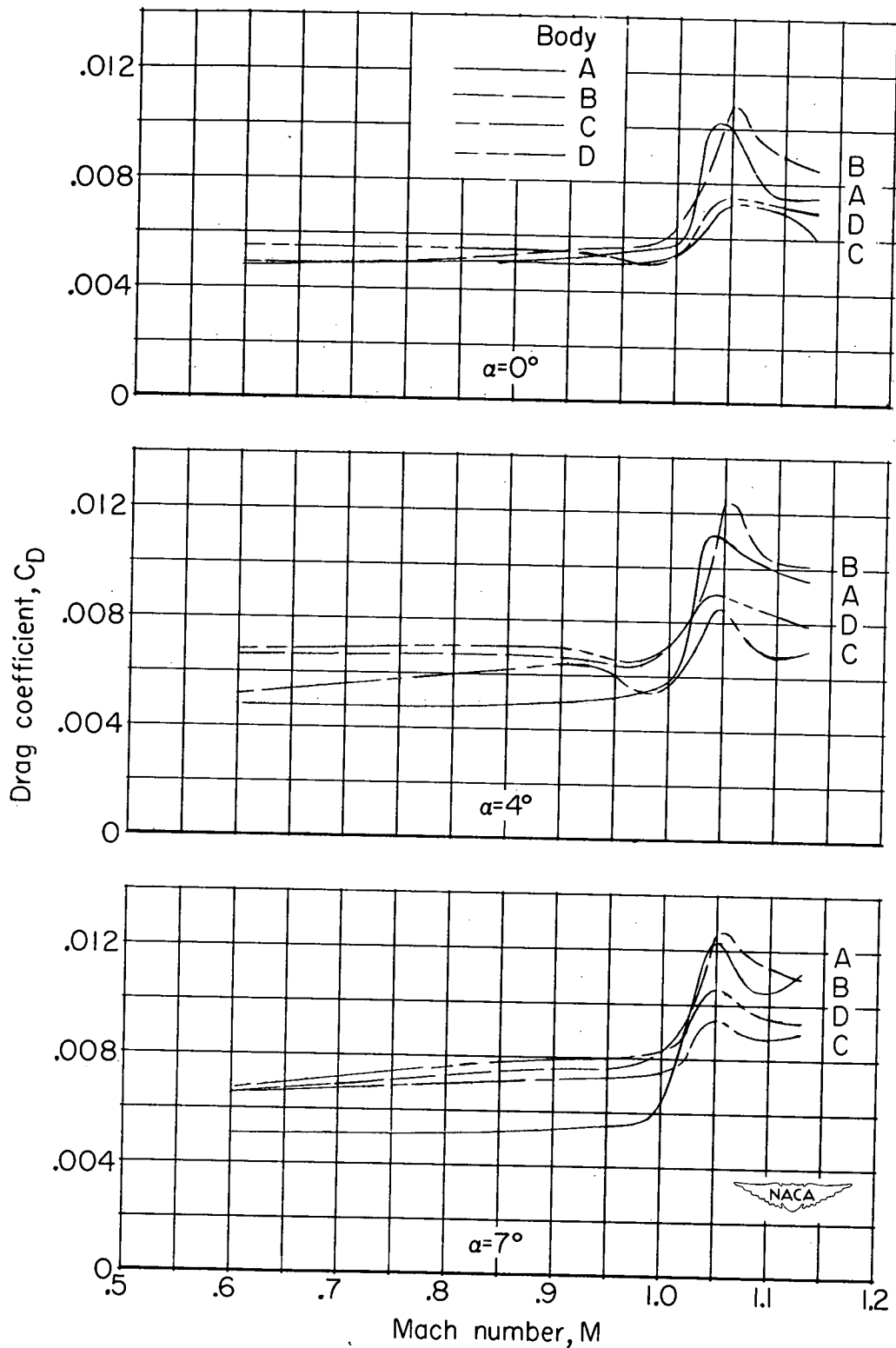


Figure 10.- Variation with Mach number of the drag coefficient of the various bodies at several angles of attack.

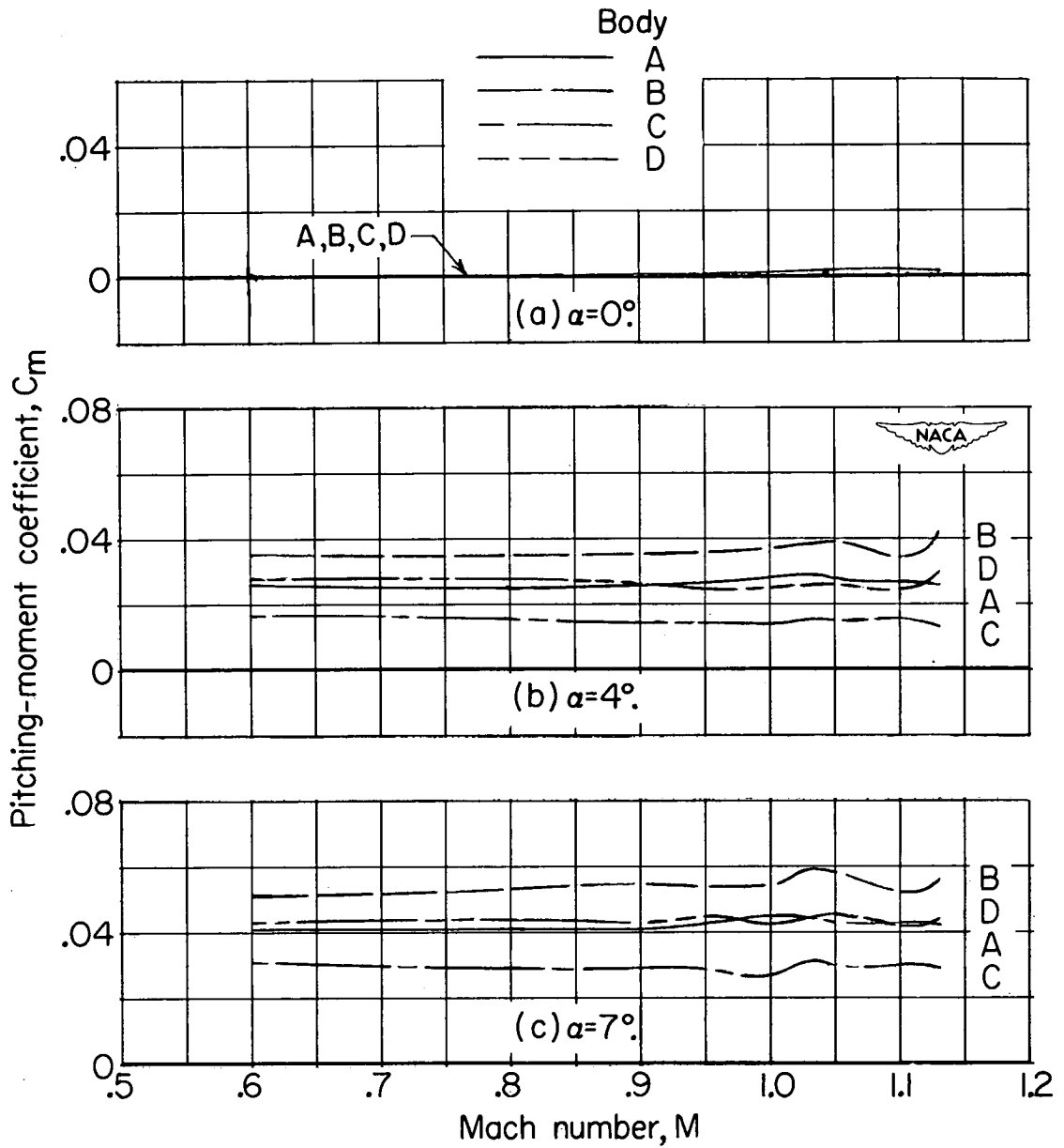
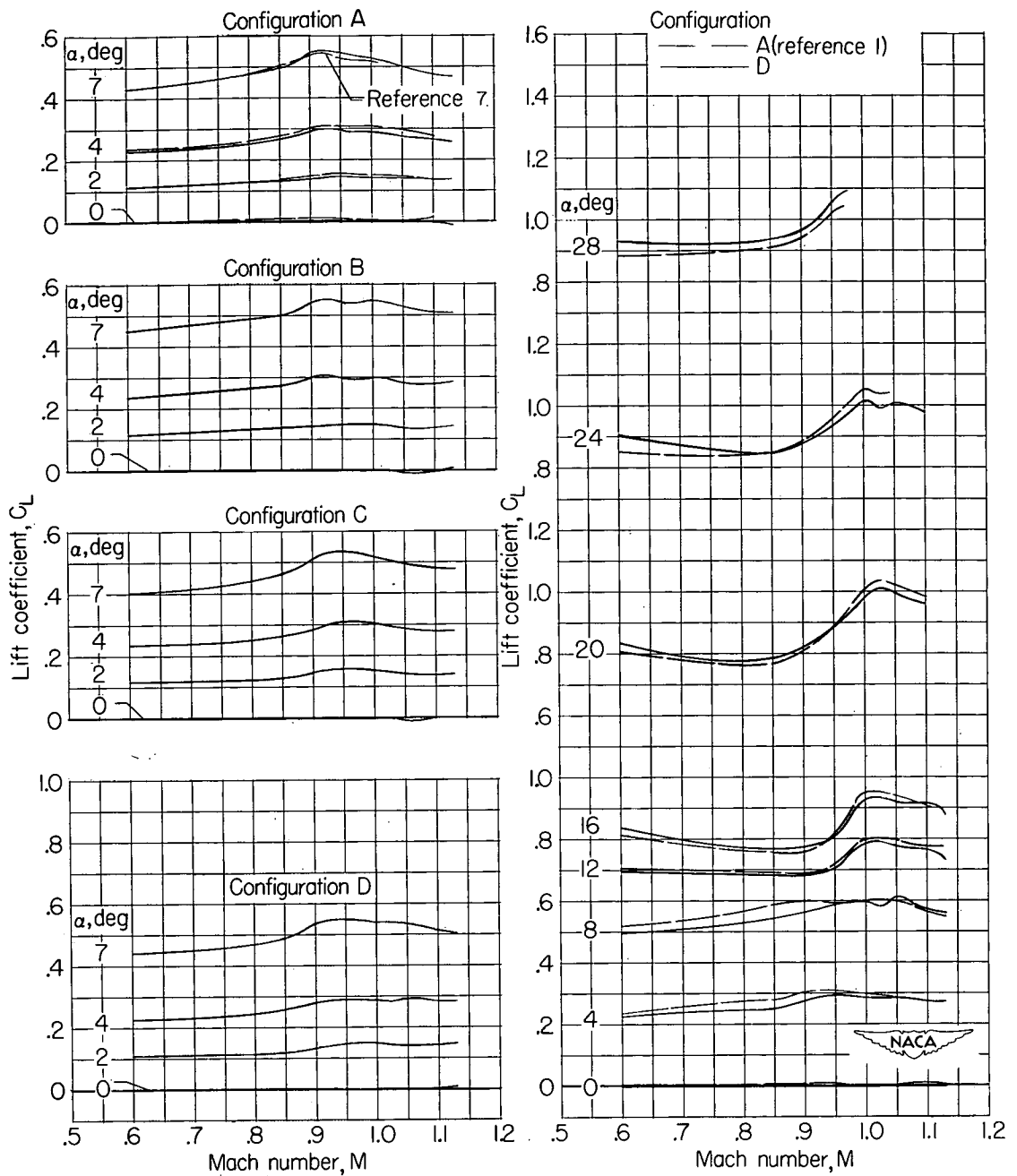


Figure 11.- Variation with Mach number of the pitching-moment coefficient of the various bodies at several angles of attack.



(a) Aluminum wing.

(b) Steel wing.

Figure 12.- Variation with Mach number of the lift coefficient of the aluminum and steel wings with interference for the various wing-body combinations at several angles of attack.

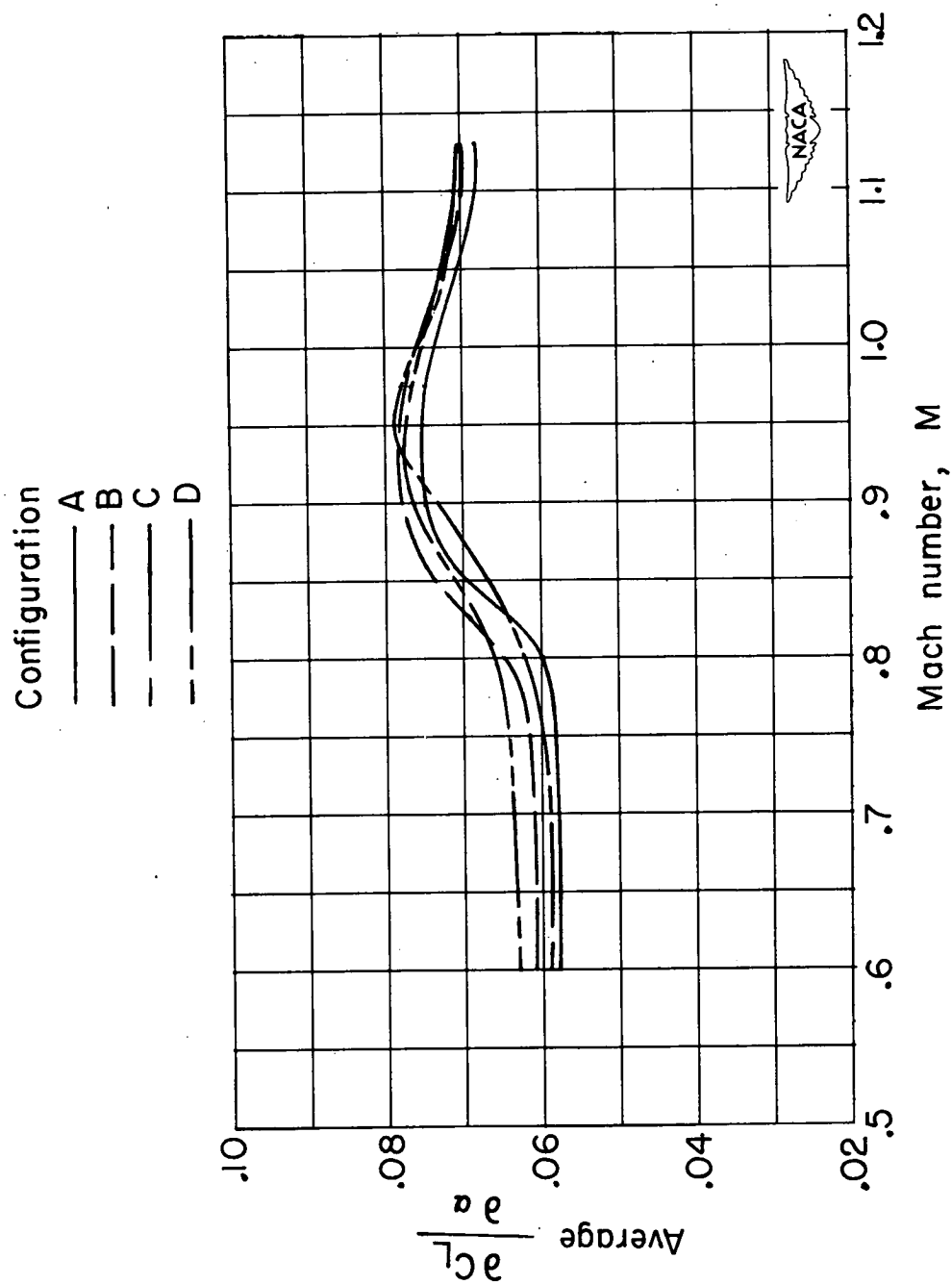


Figure 13.- Variation with Mach number of the average lift-curve slope for the aluminum wing with interference for the various wing-body combinations for an angle of attack range from 0° to 7° .

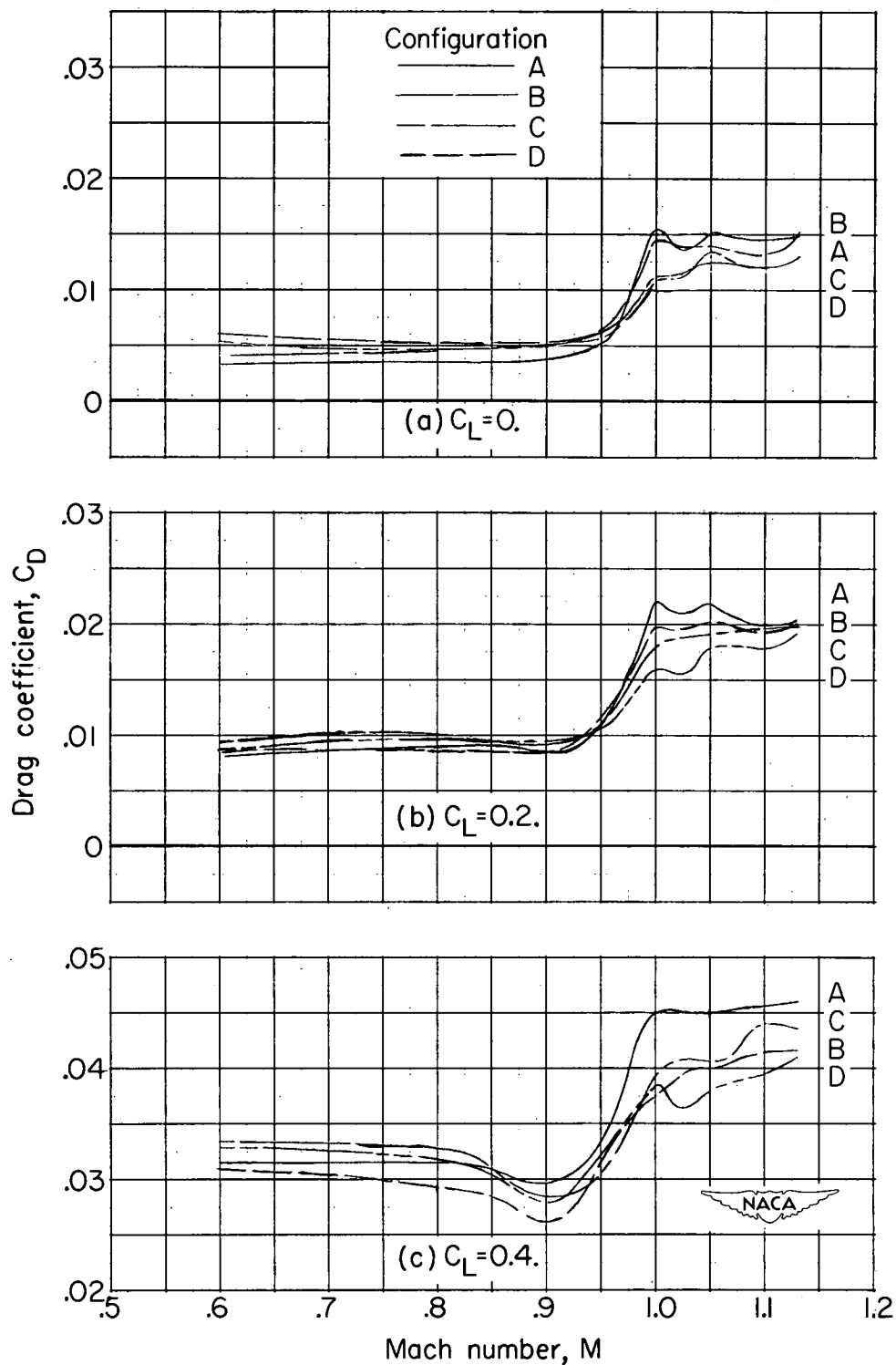


Figure 14.- Variation with Mach number of the drag coefficient of the aluminum wing with interference for the various wing-body combinations at several lift coefficients.

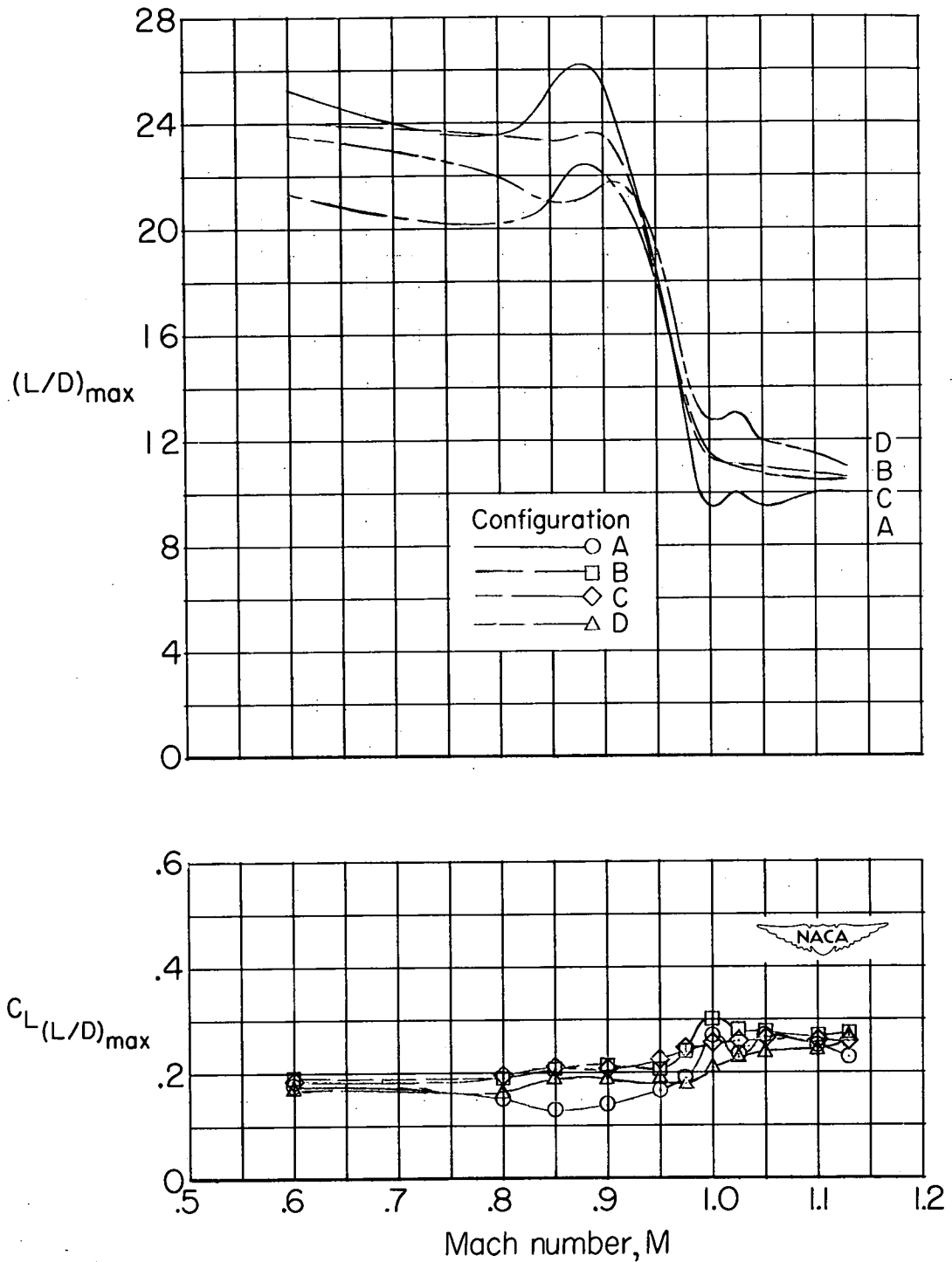


Figure 15.- Variation with Mach number of maximum lift-drag ratio and lift coefficient for the maximum lift-drag ratio for the aluminum wing with interference for the various wing-body combinations. (Symbols are included for clarity rather than to indicate test points.)

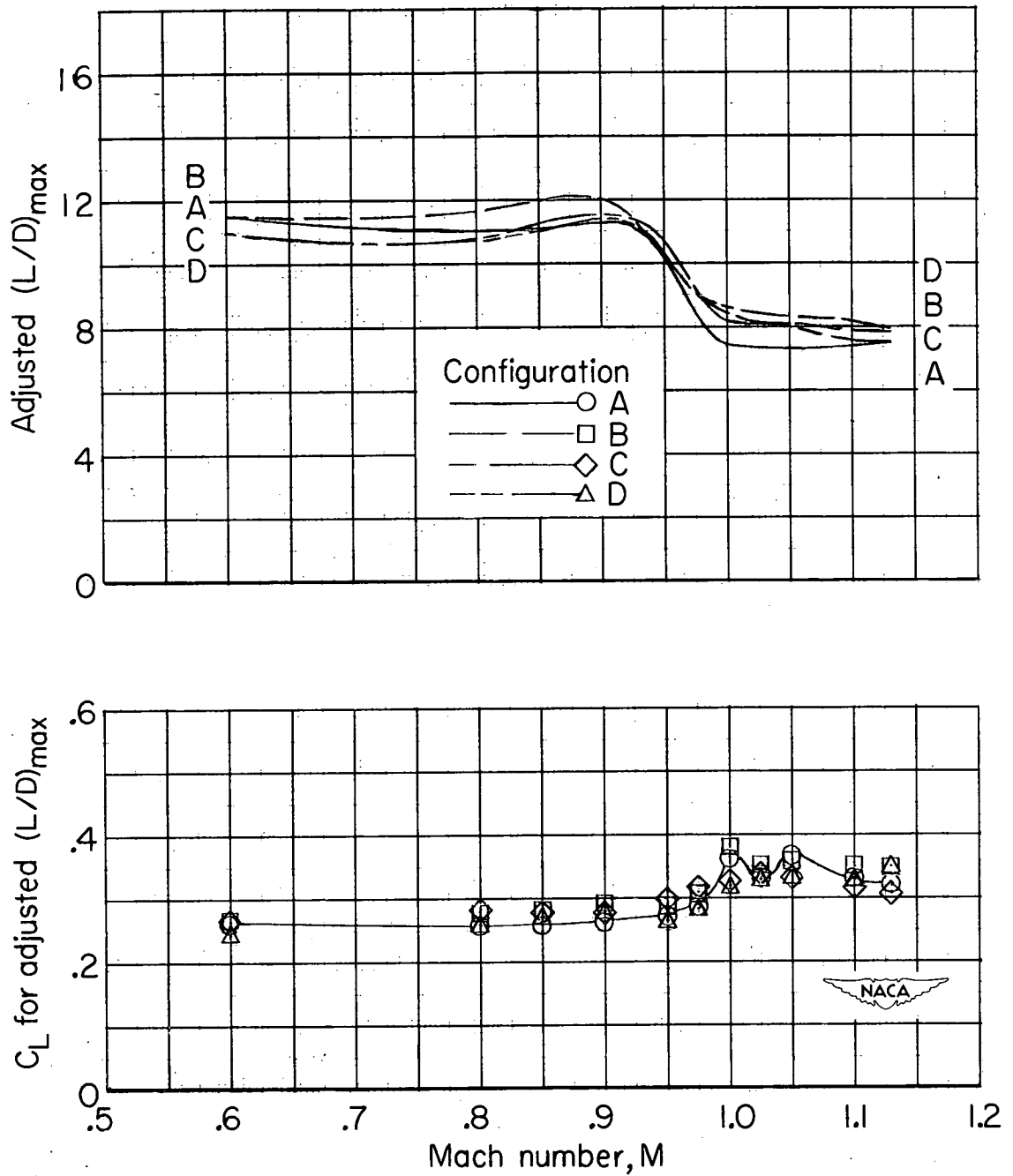


Figure 16.- Variation with Mach number of the adjusted maximum lift-drag ratio and lift coefficient for the adjusted maximum lift-drag ratio for the aluminum wing with interference for the various wing-body combinations. (Symbols are included for clarity rather than to indicate test points.)

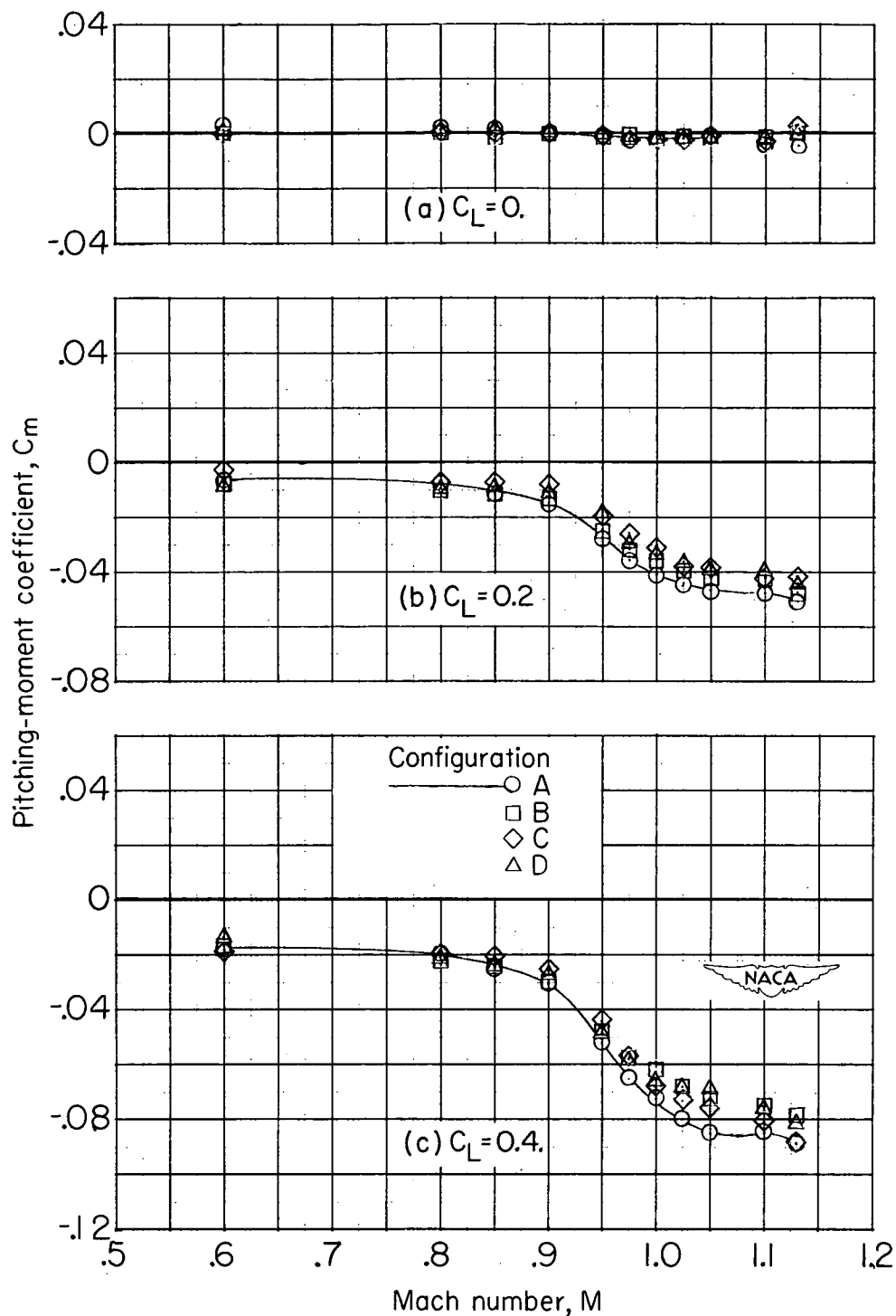


Figure 17.- Variation with Mach number of the pitching-moment coefficient of the aluminum wing with interference for the various wing-body combinations at several lift coefficients. (Symbols are included for clarity rather than to indicate test points.)